



## Volatile (Li, B, F and Cl) mobility during amphibole breakdown in subduction zones



Baptiste Debret <sup>a,\*</sup>, Kenneth T. Koga <sup>b</sup>, Fanny Cattani <sup>b</sup>, Christian Nicollet <sup>b</sup>,  
Greg Van den Bleeken <sup>b</sup>, Stephane Schwartz <sup>c</sup>

<sup>a</sup> Department of Earth Sciences, Durham University, Durham DH1 3LE, UK

<sup>b</sup> Laboratoire Magmas et Volcans, Université Blaise Pascal, CNRS, IRD, OPGC, 5 rue Kessler, 63038 Clermont Ferrand, France

<sup>c</sup> Institut des Sciences de la Terre, Université Grenoble I, CNRS, Grenoble, France

### ARTICLE INFO

#### Article history:

Received 7 July 2015

Accepted 2 December 2015

Available online 23 December 2015

#### Keywords:

Amphibole

Metagabbros

Volatile

Fluids

Subduction

### ABSTRACT

Amphiboles are ubiquitous minerals in the altered oceanic crust. During subduction, their breakdown is governed by continuous reactions up to eclogitic facies conditions. Amphiboles thus contribute to slab-derived fluid throughout prograde metamorphism and continuously record information about volatile exchanges occurring between the slab and the mantle wedge. However, the fate of volatile elements and especially halogens, such as F and Cl, in amphibole during subduction is poorly constrained. We studied metagabbros from three different localities in the Western Alps: the Chenailet ophiolite, the Queyras Schistes Lustrés and the Monviso meta-ophiolitic complexes. These samples record different metamorphic conditions, from greenschist to eclogite facies, and have interacted with different lithologies (e.g. sedimentary rocks, serpentinites) from their formation at mid-oceanic ridge, up to their devolatilization during subduction. In the oceanic crust, the initial halogen budget is mostly stored in magmatic amphibole (F = 300–7000 ppm; Cl = 20–1200 ppm) or in amphibole corona (F = 100–7000 ppm; Cl = 80–2000 ppm) and titanite (F = 200–1500 ppm; Cl < 200 ppm) formed during hydrothermal seafloor alteration. It is thus the fate of these phases that govern the halogen fluxes between the crust and the overlying mantle and/or the plate interface in subduction zones. Li and B are poorly stored in the oceanic crust (<5 ppm). In subduction zones, prograde metamorphism of metagabbros is first marked by the crystallization of glaucophane at the expense of magmatic and amphibole coronas. This episode is accompanied with a decrease of halogen concentrations in amphiboles (<200 ppm of F and Cl) suggesting that these elements can be transferred to the mantle wedge by fluids. In the Queyras Schistes Lustrés complex, the intense deformation and the abundant devolatilization of metasedimentary rocks produce large fluid flows that promote rock chemical hybridization (metasomatic mixing with hybrid composition between metasedimentary rock and metagabbro) at the metasedimentary rock/metagabbro contacts. Such fluid/rock interactions result in a strong addition of Li in glaucophane (up to 600 ppm) whereas halogen concentrations are unaffected. At eclogite facies conditions, metagabbros display low halogens concentrations (<20 ppm of F and < 100 ppm of Cl) relative to altered oceanic crust (F = 40–650 ppm; Cl = 40–1400 ppm) suggesting that these elements are continuously released by fluids during the first 30–80 km of subduction whatever the tectonic environment (e.g. slab, plate interface) and the considered fluid/rock interactions.

© 2015 Elsevier B.V. All rights reserved.

### 1. Introduction

Magmas erupted at arc volcanoes are generated by partial melting of metasomatized mantle wedge peridotites, and are enriched in H<sub>2</sub>O and volatile elements relative to Mid-Oceanic Ridge Basalts (MORB) or Oceanic Island Basalts (e.g. Le Voyer et al., 2010; Rose-Koga et al., 2014; Straub and Layne, 2003). The distinct geochemical signatures and physical properties of arc lavas result from volatile transfer from the slab to the mantle wedge (e.g. Bouilhol et al., 2009; Dalou et al.,

2012; Kendrick et al., 2012). Quantitative assessments of these chemical fluxes require knowledge about the pressure and temperature conditions at which slab-derived fluids are released and transferred to the mantle wedge and the volatile composition evolution of the slab during prograde metamorphism. Slab dehydration occurs between 40 and 200 km (e.g. Magni et al., 2014; Schmidt and Poli, 2014) and is related to the stability of hydrous phases such as serpentine (Ulmer and Trommsdorff, 1995; Wunder and Schreyer, 1997), chlorite (Grove et al., 2006, 2009), amphiboles, lawsonite, and/or mica (Pawley and Holloway, 1993; Poli and Schmidt, 1995). The evolution of volatile abundance, during the breakdown of hydrous phases in the slab, is critical to establish the mass balance of the fluxes between the slab, the

\* Corresponding author.

E-mail address: [baptiste.debret@durham.ac.uk](mailto:baptiste.debret@durham.ac.uk) (B. Debret).

surface and the deep mantle. However, it remains a significant challenge because multiple metamorphic reactions or fluid/rock interactions occur during subduction.

The composition of primitive arc magmas, recorded in olivine-hosted melt inclusions, is enriched in halogens, such as F and Cl, relative to MORB demonstrating that these elements are mobile in slab derived fluids (e.g. Le Voyer et al., 2010; Rose-Koga et al., 2014; Straub and Layne, 2003). Unlike many fluid mobile elements, such as B or Li (e.g. Bebout et al., 2007, 2013; Marschall et al., 2007, 2009; Penniston-Dorland et al., 2010, 2012; Scambelluri et al., 2004a,b; Vils et al., 2010; Zack et al., 2003; Scambelluri and Tonarini, 2012), the behavior of halogens during subduction is poorly constrained (see Kendrick et al., 2012). Halogens are present in OH<sup>-</sup> sites within hydrous minerals, such as sheet silicates or amphibole (e.g. Anselmi et al., 2000; Oberti et al., 1993; Volfingher et al., 1985). Those minerals, which are generally formed after seawater-lithosphere interactions at mid-oceanic ridges, can contain significant concentrations of halogens (up to several thousand of ppm; Barnes and Sharp, 2006; Coogan et al., 2001; Ito et al., 1983; Vanko, 1986). During prograde metamorphism, the devolatilization of serpentinites and metagabbros is accompanied with a decrease in halogen concentration suggesting that this process can trigger the transfer of a significant amount of halogens in fluids to the mantle wedge (Bonifacie et al., 2008; John et al., 2011; Kendrick et al., 2011; Philippot et al., 1998). On the other hand, Cl seems to be retained in metasedimentary rocks during subduction (Selverstone and Sharp, 2015). At depth, the devolatilization of slab serpentinites is believed to be a significant source of water and fluid mobile elements for arc magmas (e.g. Kendrick et al., 2011; Scambelluri et al., 2004a; Ulmer and Trommsdorff, 1995; Wunder and Schreyer, 1997; Scambelluri and Tonarini, 2012). However, mass balance calculation suggests that this process, alone, cannot explain the observed halogen anomalies of arc magmatism, notably F concentrations. As such additional components in the subducted oceanic lithosphere must act as significant halogen reservoirs during subduction (Debret et al., 2014).

Amphibole is a common component in the altered oceanic crust and its crystal structure can incorporate a wide range of lithophile and volatile elements (e.g. Coogan et al., 2001; Gillis et al., 2003; Messiga et al., 1995; Volfingher et al., 1985). In oceanic settings, amphibole-bearing metagabbros are formed by crystallization of silicate melt at temperature greater than 850 °C, and by continuous metamorphic reactions during lithosphere cooling and hydration between 850 to 300 °C (Coogan et al., 2001; Debret et al., 2013a; Gilbert et al., 1982; Messiga and Tribuzio, 1991; Spear, 1993; Tribuzio et al., 1995; Vanko, 1986). During subduction, amphibole breakdown in the slab is governed by continuous reactions occurring below 3 GPa (Poli and Schmidt, 1995) that release a significant amount of water (up to 2 wt%), mostly to the forearc region. It is clear that the breakdown of amphibole during subduction prograde metamorphism could be responsible for delivering a large flux of slab-derived fluid to the overlying mantle wedge. This mineral thus plays a significant role during element fractionation between the fluid and residual slab, and records continuous information about volatile transfer from slab to mantle wedge. However, while there are an increasing number of *in situ* studies focusing on the fate of volatile elements in the hydrous phases composing the subducted lithosphere (e.g. Bebout et al., 2007, 2013; Debret et al., 2013b, 2014; Lafay et al., 2013; Scambelluri et al., 2004a; Vils et al., 2010; Vitale Brovarone et al., 2014), most of them have examined micas, serpentines and/or lawsonites and the potential volatile, especially halogens, losses from amphiboles during subduction remain poorly constrained.

This study aims to determine the volatile (F, Cl, Li and B) fluxes between the different lithologies composing the slab and the mantle wedge. The approach taken is an *in situ* (Secondary ion mass spectrometry and microprobe analyses) and detailed study of amphiboles major and volatile element composition in metagabbros from a suite of Western Alps meta-ophiolites. The micro analytical methods employed here aim to separate oceanic, prograde and retrograde metamorphic evolution of

amphiboles and thus better decipher the mobility of volatile elements during metamorphism than bulk rock studies. Metagabbros from 6 different Western Alps meta-ophiolites, which metamorphic conditions span from greenschist to eclogite facies, were selected for a detailed petro-geochemical study. These samples have interacted with different lithologies (e.g. sedimentary rocks, serpentinites) during subduction leading to the released of halogens (F and Cl) to fluids.

## 2. Geological setting and petrographic observations

Western Alps meta-ophiolites represent hectometric to kilometeric size mafic and ultramafic bodies formed at magma poor settings, and are related to the opening of the Ligurian Ocean in the middle Jurassic (Lagabrielle and Cannat, 1990; Müntener et al., 2010). These meta-ophiolites represent the first few kilometers of the Ligurian oceanic lithosphere, which structure is similar to the lithosphere generated at slow- or ultra-slow spreading ridges (Bernoulli et al., 2003; Lagabrielle et al., 2014; Manatschal et al., 2011; Tricart and Lemoine, 1986). This study focuses on the Piemont zone of the south-western Alps (Fig. 1a and b) where ophiolitic units were metamorphosed and juxtaposed during alpine subduction and collision in Late Cretaceous to Tertiary (e.g. Tricart, 1984). We sampled metagabbros from 6 meta-ophiolites on a transect of ~20 km through the Queyras Schistes Lustrés complex, from the Montgenevre to the Monviso (Fig. 1b).

The studied meta-ophiolites belong to two different domains. (i) The Queyras Schistes Lustrés complex consists of 10% of meta-ophiolites and 90% of metasedimentary rocks and is interpreted as a paleo-sedimentary wedge (Tricart and Schwartz, 2006). The Queyras meta-ophiolites form metric to kilometeric bodies embedded in dominant Jurassic to Lower Cretaceous clastic metasedimentary rocks (Lagabrielle et al., 1984; Lemoine et al., 1987). They have experienced strong interactions between mafic lithologies and sediment derived fluid during subduction (Lafay et al., 2013). In this complex, three tectono-metamorphic units record variable P-T conditions (Fig. 1b, c), increasing from low-temperature blueschist facies conditions (LT-blueschist; 320–360 °C and 9–11 kbar) in western Queyras to medium-temperature (MT-blueschist; 340–390 °C and 10–12 kbar) and high-temperature blueschist (HT-blueschist; 380–470 °C and 12–18 kbar) conditions toward to the East (Agard et al., 2001; Ballèvre et al., 1990; Lagabrielle et al., 2014; Schwartz et al., 2013; Tricart and Schwartz, 2006). (ii) The Monviso meta-ophiolite corresponds to a remnant of the oceanic lithosphere preserving multiple slices of the oceanic crust embedded in serpentinites and re-equilibrated at eclogitic facies P-T conditions (Angiboust et al., 2011; Schwartz et al., 2001). Unlike the Queyras meta-ophiolites, the massif evolved during subduction without interacting with external fluids (Lafay et al., 2013).

For reference, we also studied the Chenaillet massif. This massif is considered to be representative of the pre-subduction alpine oceanic lithosphere since it has been poorly affected by alpine subduction/collision and related metamorphism (e.g. Caby, 1995; Lafay et al., 2013; Lagabrielle et al., 2014; Manatschal et al., 2011; Mével et al., 1978; Schwartz et al., 2013). The massif is interpreted as an obducted portion of the Tethyan oceanic lithosphere (e.g. Caby, 1995). It preserves a complete section of the oceanic lithosphere composed of serpentinite intruded by metagabbros and topped by basalts and rare sediments (Manatschal et al., 2011). The massif mostly records an oceanic metamorphism, ranging from granulite to greenschist facies conditions, during lithosphere cooling and hydration (Mével et al., 1978).

### 2.1. The Chenaillet ophiolite

The Chenaillet ophiolite (Fig. 1b) is a thin tectonic nappe resting upon the Queyras Schistes Lustrés complex. The massif preserves pre-Alpine structure and basement-cover relationship between serpentinitized mantle, metagabbros, sediments and metabasalts. The

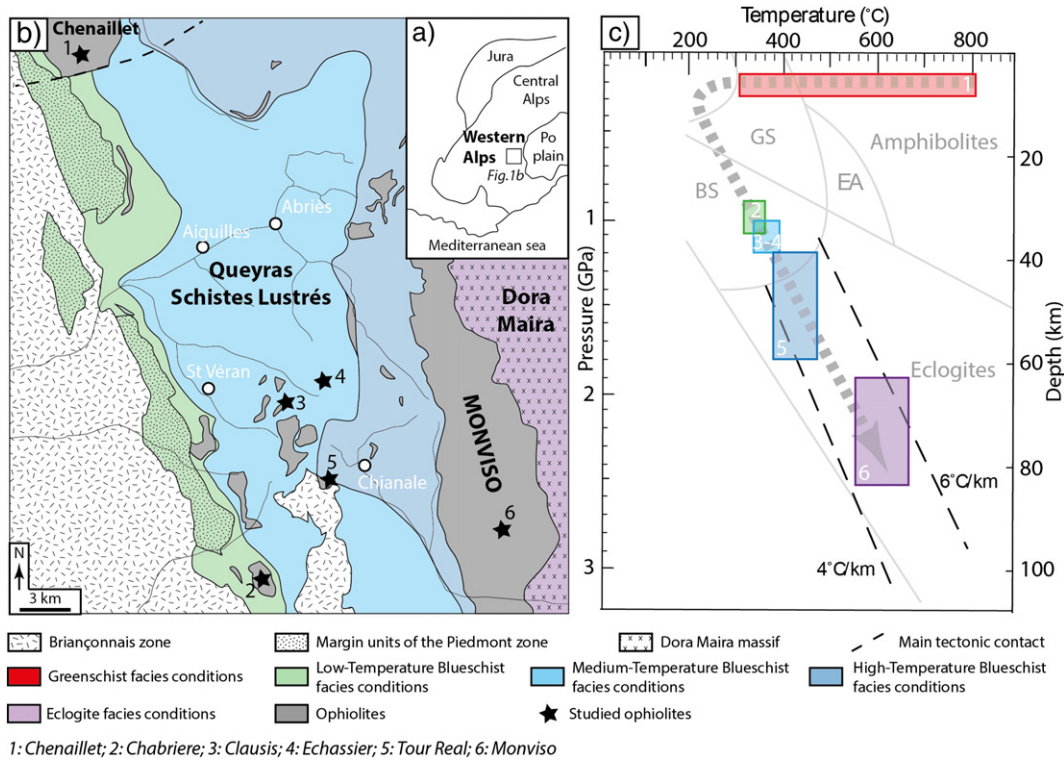


**Fig. 1.** (a) Map of the Western Alps indicating the location of the studied area. (b) Metamorphic map of the studied area showing the locations of the studied ophiolites. (c) Pressure and temperature estimates of the studied ophiolites. Modified after Schwartz et al. (2013).

metagabbroic pods are less than 1 km in diameter and show coarse-grained textures. Locally, they show porphyroclast stretching and foliation (Fig. 2a) characterizing a post-magmatic deformation during

cooling (e.g. Debret et al., 2013a). They are composed of clinopyroxene, plagioclase, ilmenite, Ti-magnetite, low pressure-amphiboles (LP amphiboles), titanite, chlorite, albite and epidote.

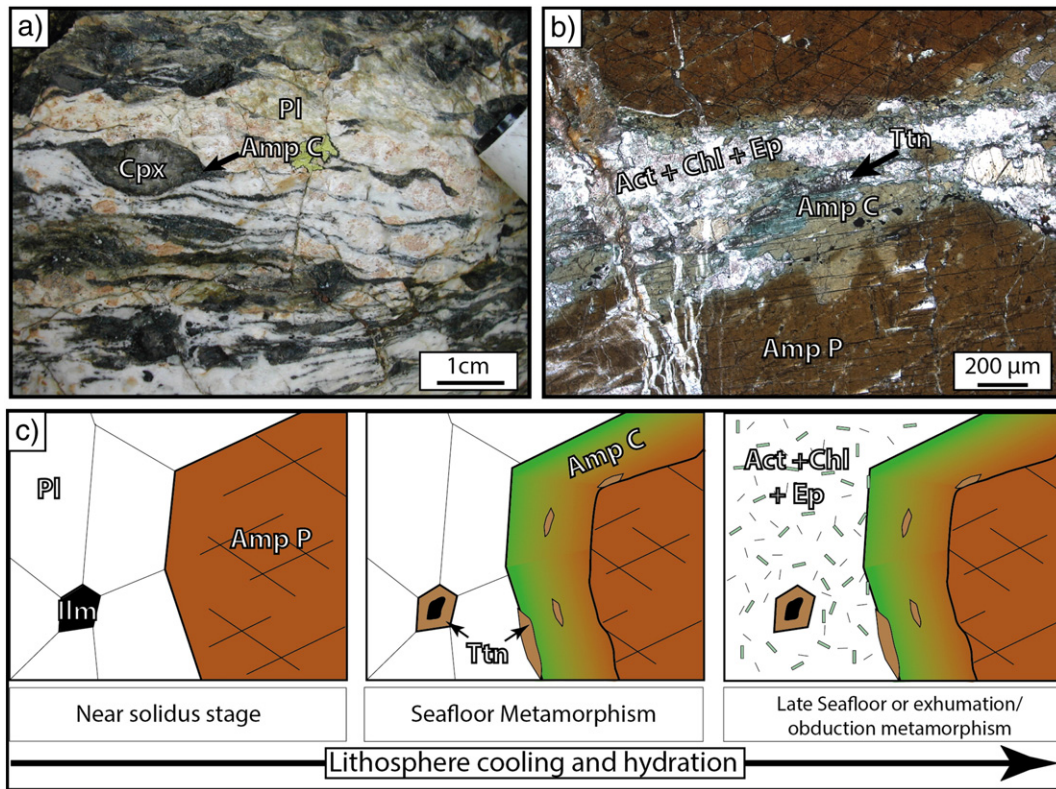


**Fig. 2.** (a) Foliated metagabbro of the Chenaillet ophiolite displaying clinopyroxene porphyroclasts surrounded by thin black coronas of amphibole. (b) Photomicrographs of metagabbro from the Chenaillet ophiolite showing amphibole porphyroclasts (Amp P) partly recrystallized into amphibole coronas (Amp C). The amphibole coronas are zoned from light brown to green toward the rims. (c) Schematic diagram showing the sequence of amphibole crystallization during lithosphere cooling and hydration.

Based on petrographic observations, three different generations of amphiboles can be distinguished in Chenaillet metagabbros. These amphiboles will be referred as (1) amphibole porphyroclasts, (2) amphibole coronas and (3) actinolites in the rest of the paper (Fig. 2b, c). (1) Amphibole porphyroclasts correspond to melt derived brown amphiboles crystals of 0.5 mm to 1 cm width displaying planar grain boundaries (Fig. 2b, c). (2) Amphibole coronas are formed during the cooling and hydration of the lithosphere on the seafloor. They partly to fully replace magmatic clinopyroxene or amphibole porphyroclasts and display an optical zoning from brownish-green to green toward to porphyroclast rims (Fig. 2b, c). Amphibole coronas contain titanite inclusions of ~20 µm width. (3) Actinolites are concentrated in the plagioclase domain or at the rims of amphibole or clinopyroxene porphyroclasts. They are associated with small grains of chlorite, albite and/or epidote needles of <50 µm width (Fig. 2b, c). The formation of these assemblages can be related to late seafloor or obduction/exhumation metamorphism. Some ilmenites crystallize as irregular interstitial grains of 200–500 µm width within plagioclase and clinopyroxene domains. They are surrounded by a titanite corona of ~100 µm width. Rare magmatic olivines are replaced by tremolite and chlorite aggregates.

## 2.2. The Queyras Schistes Lustrés complex

The Queyras Schistes Lustrés complex (Fig. 1b) is composed of metamorphosed Mesozoic oceanic sediments, which have been strongly deformed during alpine subduction. The complex includes boudinaged units of serpentinites, metagabbros and metabasalts from meter to kilometer size that can be associated with their original sedimentary cover (Lagabriele and Polino, 1988; Tricart and Lemoine, 1986). The Queyras metagabbros record various blueschist facies P-T conditions (Fig. 1b, c). They are mainly composed of magmatic clinopyroxene relics, LP-amphibole, ilmenite, titanite, glaucophane, lawsonite, chlorite, +/- albite, +/- epidote and +/- quartz. In these rocks, textural relationships show that glaucophane and lawsonite (+/- epidote, quartz) replaced LP amphiboles and the plagioclase domain.

The Chabrière meta-ophiolite (Fig. 1a) is a hectometric massif embedded within metasedimentary rocks, and composed of pillow lavas, metadiorites, metagabbros and serpentinites. The metagabbros show coarse-grained textures and locally display a magmatic deformation characterized by porphyroclast stretching and a foliation. They record LT-blueschist facies P-T conditions (300–350 °C, 8–11 kbar; Fig. 1c). Within these rocks the oceanic LP-assemblages are well preserved. They are composed of clinopyroxene, amphibole porphyroclast, amphibole corona, actinolite and interstitial ilmenite surrounded by titanite corona (Fig. 3a). At the contact of the plagioclase domain, LP-amphiboles are partly recrystallized into glaucophane forming coronas of ~300 µm width (Fig. 3a). The plagioclase domain is fully recrystallized into elongated crystals of lawsonite up to ~50 µm long and interstitial albite (Fig. 3a).

The Clausis meta-ophiolite (Fig. 1b) is a hectometric body composed of metagabbroic and serpentinite boudins recording M-T blueschist facies conditions (340–390 °C, 10–12 kbar; Fig. 1c). The contact between metasedimentary rocks and metagabbros is marked by quartzite veins composed of coarse quartz, glaucophane and small titanite grains. In these metasomatic zones, the glaucophane displays idiomorphic textures suggesting that it is in equilibrium with quartz. In the metagabbros, the clinopyroxene and the LP-amphiboles are poorly preserved. Glaucophane coronas of 100–300 µm width replace the amphibole coronas and contain titanite inclusions of 50 µm width, whereas glaucophanes crystallizing in plagioclase domain are titanite free (Fig. 3b). The plagioclase domain is finely recrystallized into lawsonite, +/- phengite, zoisite and quartz crystals of less than 50 µm width. Retrograde epidote and albite have been observed at the contact between lawsonite and glaucophane (Fig. 3b). As previously observed, interstitial ilmenites are surrounded by titanite coronas.

The Echassier meta-ophiolite is located to the East of the Clausis meta-ophiolite. Both massifs record similar P-T conditions (Schwartz

et al., 2013). The Echassier meta-ophiolite is composed of hectometric serpentinite and metagabbroic pods and rare metabasalts embedded within metasedimentary rocks. Metagabbros display coarse-grained texture and similar metamorphic assemblages to that of Clausis metagabbros. The contact between metagabbros and metasedimentary rocks is characterized by metasomatic zones composed of interstitial calcite and chlorite and randomly orientated tremolite and diopside needles of 50 µm long. At the contact of these zones, we have sampled a metabasalt which has been finely recrystallized into idiomorphic glaucophane and chlorite of 100 µm width with interstitial calcite and small aggregates of titanite (Fig. 3c, d).

The Tour Real meta-ophiolite is located to the East of the study area and is metamorphosed at HT-blueschist facies conditions during subduction (380–470 °C, 12–18 kbar; Fig. 1b, c). It represents a kilometric segment of oceanic lithosphere and is characterized by metagabbroic pods embedded in serpentinites. The contact between metagabbros and serpentinites is composed of fibrous serpentine associated with titanite and chlorite. We sampled glaucophane bearing shear zone crossing metagabbros (Fig. 3e). These rocks are characterized by the absence of LP amphiboles. They are composed of clinopyroxene porphyroclasts of ~200 µm width surrounded by glaucophane coronas of 200 µm width (Fig. 3f). The plagioclase domain is fully recrystallized into lawsonite, epidote, magnetite and chlorite. The preferential crystallization of hydrous phases in these shear zones, relative to the host rock, suggests that these zones localized fluid circulation during subduction.

## 2.3. The Monviso meta-ophiolite

The Monviso meta-ophiolite is located in the extreme east of the study area (Fig. 1b) and is separated from the Queyras Schist Lustrés complex by a ductile normal fault (Ballèvre et al., 1990). This meta-ophiolite extends over 30 km and is composed of hectometric lenses of metabasites embedded within highly deformed serpentinites with rare metasedimentary rocks (Angiboust et al., 2011; Lombardo et al., 1978; Schwartz et al., 2001). The massif records various eclogite facies metamorphic conditions with a maximum P-T estimated at 550–620 °C and 1.9–2.6 GPa (Angiboust et al., 2011; Schwartz et al., 2001). The massif consists primarily of metagabbros and serpentinites with few metasedimentary rocks (<10%) relative to the Queyras Schiste Lustrés complex. The metagabbros display heterogeneous deformation, which is characterized by porphyroclast stretching and the formation of bandings. Relative to blueschist facies metagabbros from the Queyras, the eclogitic metagabbros of the Monviso meta-ophiolite are characterized by a low abundance of glaucophane (less than 10%), the absence of titanite and lawsonite, and the crystallization of idiomorphic garnet, omphacite, quartz, small rutile grains of ~20 µm in width, and +/- phengite and zoisite (Fig. 4).

## 3. Methods

### 3.1. Sample preparation

Standard thin sections of 30 µm thickness were prepared from hand samples. After detailed petrographic description, areas of approximately 2 by 2 mm size were selected and cut out of the thin sections. These areas contain mineral assemblages that are representative of the main stages of metagabbro recrystallization during prograde metamorphism. Typically, ten to twelve pieces were placed on a single mount filled with indium. This technique minimizes the number of sample changes during analyses and contributes to better analytical stability. Laboratory synthesized glasses, doped with in F and Cl, were also inserted into every mount and used to monitor for machine drift. Gold coating was used for IMS 1270 SIMS analyses, and carbon coating for IMS 7f and electron microprobe analysis. In order to avoid multiphase analyses, optical microscope and SEM images were used to identify minerals in the thin section and to select spots for SIMS analyses. After to the

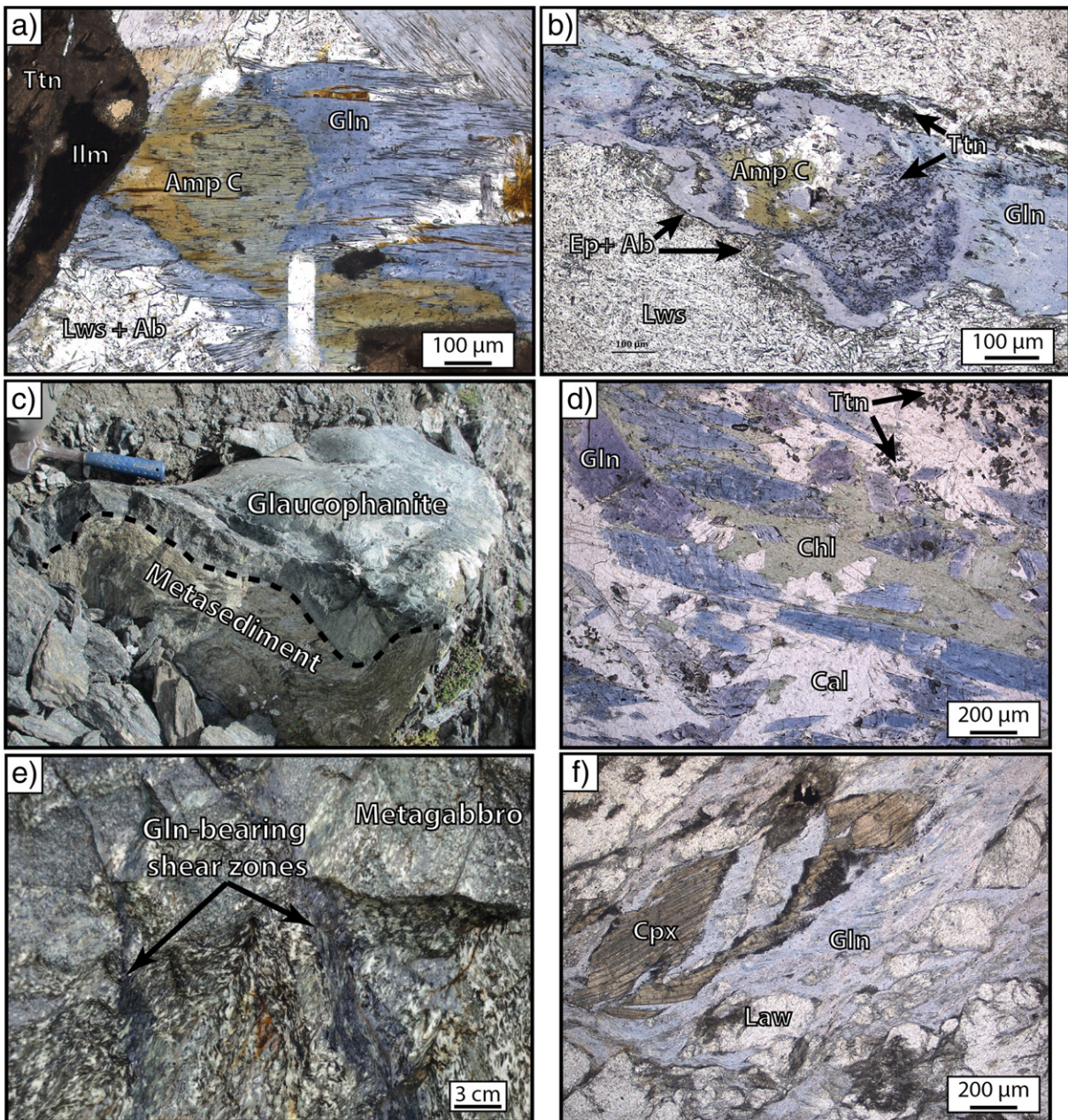


**Fig. 3.** Photomicrographs under plane polarized light (a, b, d, f) and photo (c, e) of metabasite from the Queyras Schistes Lutres complex. (a) Metagabbro from Chabrière ophiolite displaying a zoned amphibole corona partly recrystallized into glaucophane. The ilmenite is surrounded by a titanite corona. (b) Metagabbro from Clausis ophiolite showing glaucophane surrounding an amphibole corona. Small titanite grains are included in the glaucophane replacing the amphibole corona. Epidote crystallizes at the contact between glaucophane and lawsonite. (c–d) Metasomatic glaucophanite crystallizing at the contact between metagabbroic pods and metasedimentary rocks. It is composed of idiomorphic glaucophane and chlorite and interstitial calcite; Echassier ophiolite. (e–f) Glaucophane bearing shear zones crossing metagabbroic pods of Tour Real ophiolite. These zones are composed of glaucophane and lawsonite. The glaucophane can locally surround kink-banded clinopyroxene.

SIMS analyses, we performed microprobe analyses to ensure correct mineral phase was analyzed.

### 3.2. Electron microprobe

Major element analyses of metagabbroic minerals have been performed with a Cameca SX100 at the Laboratoire Magmas et Volcans (Clermont-Ferrand, France). The primary acceleration voltage was 15 kV, and a 15 nA beam current was used for all mineral analyses. Amphiboles with high F and Cl concentrations were also measured by electron microprobe. To avoid Fe peak interference on the light element detector, three thallium acid phthalate crystals were used to simultaneously measure F for a 300 s total counting time. A pentaerythritol

crystal was used for Cl measurements for 100 s counting time. The machine was calibrated with a  $\text{CaF}_2$  and a scapolite. KE12 glass was used as an external standard. The detection limits of this procedure are about 350 and 60 ppm for F and Cl, respectively.

### 3.3. Secondary ion mass spectrometer

A Cameca IMS 1270 at CRPG (Nancy, France) was used to determine the concentrations of F and Cl. Measurements were conducted with a  $\sim 10 \mu\text{m}$  beam size for all analyses, using a  $\text{Cs}^+$  primary beam with primary and secondary accelerating voltage of 10 kV, and no energy offset was applied.  $^{19}\text{F}$ ,  $^{35}\text{Cl}$ ,  $^{31}\text{P}$  and  $^{32}\text{S}$  measurements were obtained with an electron multiplier. Backgrounds were measured at mass 17.5. A high

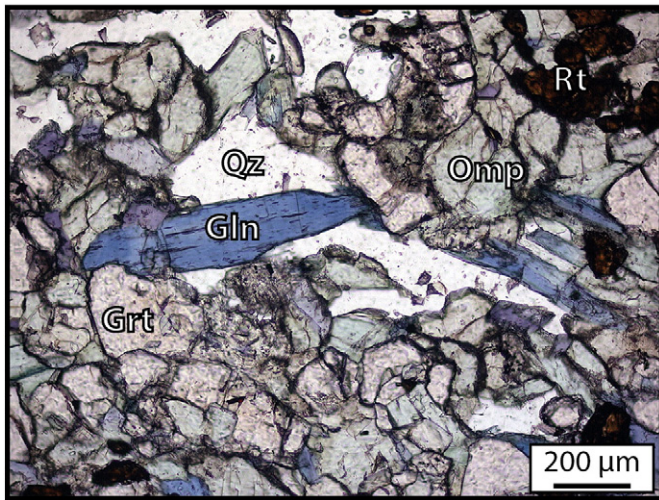


Fig. 4. Eclogite from the Monviso ophiolite displaying an equilibrium paragenesis composed of glaucophane, garnet, omphacite, quartz and rutile.

mass-resolution (MRP = 3000 minimum) was set to separate major molecular interferences.  $^{28}\text{Si}$ ,  $^{18}\text{O}$  and  $^{17}\text{S}$  measurements were obtained with a Faraday cup. Each analysis consists of 10 cycles.  $^{17}\text{S}$ ,  $^{18}\text{O}$ ,  $^{19}\text{F}$ ,  $^{28}\text{Si}$ ,  $^{31}\text{P}$ ,  $^{32}\text{S}$ , and  $^{35}\text{Cl}$  were counted for 4 s each, with 1 or 2 s waiting time. The intensity measured at masses  $^{19}\text{F}$ ,  $^{35}\text{Cl}$  and  $^{32}\text{S}$  were normalized to  $^{18}\text{O}$ . Signals of P and S were often weak and erratic; we did not report these data in this study. The F and Cl contents were determined by measuring international glass standards and laboratory standards (ML3B, ATHO, T1g, Alv2390, and KE12; Appendix A for calibration and see Van den Bleeken and Koga, 2015, for long term reproducibility and matrix issues). As reported in Debret et al. (2014), we found that  $^{18}\text{O}$  referenced calibration curves provide coherent and reproducible fits among mixed standard samples instead of Si. Our compilation of standard analyses indicates that O signal variability was about 20% less than that of Si normalization.

Table 1  
Main assemblages composing the studied metagabbros.

Sample name	Location	Lithology	Main mineral assemblages	
			LP metamorphism	Alpine HP metamorphism
Ch1	Chenaillet	Deformed metagabbro	Cpx–amphibole coronas–actinolite–albite–epidote–chlorite–ilmenite–titanite	
Ch5		Meta-dolerite	Cpx–amphibole porphyroclasts–amphibole coronas–actinolite–albite–epidote–chlorite–ilmenite–titanite	
Ch3		Amphibolite	Amphibole porphyroclasts–amphibole coronas–actinolite–albite–epidote–ilmenite–titanite	
Ch10		Amphibolite	Amphibole porphyroclasts–amphibole coronas–actinolite–albite–epidote–ilmenite–titanite	
QE32	Chabriere	Meta-diorite	Cpx–ilmenite <sup>±</sup> –apatite–titanite–amphibole porphyroclasts–amphibole coronas–actinolite	Glaucophane–lawsonite–albite–actinolite
QE33		Meta-dolerite	Ilmenite–titanite–amphibole coronas–actinolite	Glaucophane–lawsonite–albite <sup>±</sup> –zoisite
QE34		Metagabbro	Ilmenite–titanite–amphibole coronas <sup>±</sup> –apatite	Glaucophane–lawsonite–albite
QE6	Clausis	Metagabbro	Amphibole coronas–titanite	Glaucophane–lawsonite <sup>±</sup> –albite–zoisite–quartz–calcite
QE9		Metagabbro	Cpx–amphibole coronas–actinolite–ilmenite–titanite	Glaucophane–lawsonite
CI2		Metagabbro	Cpx–ilmenite–titanite	Glaucophane–lawsonite <sup>±</sup> –epidote
Q13		Metasomatic quartzite		Quartz–glaucophane–titanite–stiplomelane
CE8	Echassier	Metasomatic glaucophanite		Glaucophane–calcite–chlorite–titanite <sup>±</sup> –ilmenite
TR11	Tour Real	Fracture in a metagabbro	Cpx	Glaucophane–lawsonite–zoisite–chlorite–magnetite
TR16		Shear zone in metagabbro	Cpx	Glaucophane–zoisite
QE29d	Monviso (Verne)	Eclogite		Omphacite–garnet–glaucophane–quartz–rutile <sup>±</sup> –Phengite
Gala	Monviso (Passo Gallarino)	Eclogite		Omphacite–garnet–glaucophane–quartz–Rutile <sup>±</sup> –Phengite

A Cameca IMS 7f at Institut Jean Lamour (Nancy, France) was used for concentration measurements of Li and B. A primary beam of  $\text{O}_2^-$  was accelerated to 10 kV, no energy filtering was used, and a 40 eV width energy window was centered around 0 offset. The size of primary beam was approximately 30  $\mu\text{m}$ . The intensity was measured at masses  $^6\text{Li}$ ,  $^{11}\text{B}$ , and  $^{28}\text{Si}$ , for 1, 5 and 1 s counting time, respectively. An electron multiplier was used for  $^6\text{Li}$  and  $^{11}\text{B}$ , and a faraday cup was used for  $^{28}\text{Si}$ . Each analysis consists of 20 cycles. Linear concentration calibration curves were established using NIST standards (NBS 610, 612, 614, and 616, see Appendix B for calibration).

#### 4. Mineral chemistry

A set of 16 metagabbros were selected as they were considered representative of metamorphic mineral reactions occurring during crust cooling and hydration in oceanic setting and prograde subduction zone metamorphism (Table 1). Major element compositions of minerals are reported in Table C1, volatile (F, Cl, Li and B) abundances are listed in Table 2.

##### 4.1. Oceanic assemblages of Chenaillet metagabbros

To constrain the behavior of volatiles during oceanic crust cooling and hydration, 4 samples from the Chenaillet ophiolite preserving LP-parageneses have been analyzed (Table 1). The magmatic paragenesis is composed of clinopyroxene, plagioclase, ilmenite and amphibole. The magmatic clinopyroxenes are diopside in composition and are characterized by  $X_{\text{Mg}}$  ( $= \text{Mg}/[\text{Mg} + \text{Fe}]$  in mol fraction) ranging from 0.76 to 0.83 and CaO and  $\text{Al}_2\text{O}_3$  contents varying from 21.3 to 24.6 wt% and 0.35 to 3.1 wt%, respectively. Magmatic amphibole porphyroclasts display an edenite composition characterized by  $\text{TiO}_2$  and  $\text{Al}_2\text{O}_3$  contents ranging from 2.5 to 4 wt% and from 7 to 11 wt% respectively. Amphibole coronas display lower  $\text{TiO}_2$  ( $= 0.2\text{--}2.1$  wt%) and highly variable  $\text{Al}_2\text{O}_3$  ( $= 2\text{--}13$  wt%) contents relative to amphibole porphyroclasts (Fig. 5). Their compositions vary from Mg- or Fe-hornblende to edenite. Amphibole coronas commonly present a  $\text{TiO}_2$  zoning decreasing toward crystal rims. Titanite inclusions in amphibole coronas or surrounding

Table 2

SIMS analyses of pyroxene, amphibole, titanite, ilmenite, lawsonite, epidote, chlorite, rutile, omphacite, garnet, quartz and phengite.  $2\sigma$  corresponds to the analytical uncertainty.

Massif	Sample	F	$2\sigma$	Cl	$2\sigma$	B	$2\sigma$	Li	$2\sigma$
<i>Pyroxene</i>									
CHE	Ch1.3	3.7	0.6	68	6	2.1	0.1	2.07	0.04
TR	TR11.3	23.9	0.7	63	6	2.6	0.2	16.4	0.7
TR	TR11.3	18.8	1.0	44	5	3.0	0.2	31.2	1.6
TR	TR16.3	15.8	0.4	33	5	2.3	0.2	18.6	0.7
TR	TR16.2	12.9	0.4	39	6	1.0	0.2	6.1	0.3
TR	TR16.1	13.9	0.6	40	4	0.8	0.2	3.1	0.3
<i>Amphibole porphyroclasts</i>									
CHE	Ch3.1	1285	5	89	3	2.7	0.2	0.40	0.07
CHE	Ch3.2	1624	15	128	20	2.5	0.3	0.5	0.1
CHE	Ch3.3	1583	7	249	37	3.2	0.2	0.5	0.1
CHE	Ch3.3	1710	8	197	10	3.3	0.3	0.6	0.1
CHE	Ch3.4	1368	16	91	7	1.6	0.1	0.4	0.1
CHE	Ch3.4	1331	14	113	6	2.5	0.2	0.4	0.1
CHE	Ch3.5	1279	22	140	13	3.3	0.3	1.0	0.2
CHE	Ch3.5	1225	11	126	19	2.5	0.2	0.5	0.2
CHE	Ch5.1	2011	13	280	4	5.3	0.2	1.09	0.05
CHE	Ch5.1	1386	15	112	7	0.52	0.12	0.20	0.05
CHE	Ch5.2	1557	10	19	2	0.29	0.06	0.03	0.02
CHE	Ch5.2	1636	9	20	2	1.0	0.1	0.6	0.2
CHE	Ch5.2	1208	5	52	7	0.48	0.07	0.20	0.06
CHE	Ch5.4	1401	14	90	11	1.98	0.10	2.1	0.5
CHAB	QE32.1	381	2	1224	12	2.6	0.1	15.4	0.6
CHAB	QE32.1	281	5	35	7	6.8	0.2	36.2	1.1
CHAB	QE32.2	283	3	348	8	1.4	0.1	1.2	0.2
CHAB	QE33b.3	7123	56	206	13	2.0	0.2	11.6	0.1
<i>Amphibole coronas</i>									
CHE	Ch1.1	862	3	772	38	34.1	0.7	0.4	0.1
CHE	Ch1.1	886	8	770	67	30.1	0.6	0.62	0.07
CHE	Ch1.1	848	5	569	102	27.6	0.3	1.33	0.08
CHE	Ch1.1	612	5	434	42	15.7	0.2	0.44	0.07
CHE	Ch1.1	N.D.	N.D.	267	25	10.5	0.3	0.58	0.07
CHE	Ch1.1	N.D.	N.D.	386	54	8.0	0.3	0.78	0.06
CHE	Ch1.1	N.D.	N.D.	410	54	11.8	0.4	0.45	0.05
CHE	Ch1.3	270	3	1708	42	2.5	0.3	0.7	0.1
CHE	Ch1.3	419	5	416	8	27.5	0.4	0.63	0.06
CHE	Ch1.3	417	8	447	7	26.0	0.5	5.9	0.4
CHE	Ch1.3	384	13	372	10	26.5	0.4	0.9	0.1
CHE	Ch3.1	1973	15	126	6	4.4	0.4	3.8	0.5
CHE	Ch3.2	1502	23	104	4	2.0	0.1	0.16	0.02
CHE	Ch3.2	749	6	79	5	2.1	0.3	4.9	0.8
CHE	Ch3.2	271	7	133	7	2.7	0.2	1.8	0.3
CHE	Ch3.3	740	9	156	10	2.4	0.2	0.22	0.05
CHE	Ch3.4	1803	8	119	4	2.6	0.2	0.9	0.2
CHE	Ch3.4	1399	11	139	20	1.5	0.1	0.17	0.04
CHE	Ch3.4	113.5	1.1	164	11	2.6	0.3	3.6	0.8
CHE	Ch3.5	340	2	975	81	3.1	0.2	0.9	0.2
CHE	Ch5.1	86.0	0.8	169	3	0.57	0.13	0.52	0.07
CHE	Ch5.1	100.9	0.9	156	5	0.3	0.1	0.10	0.01
CHE	Ch5.2	360	4	1357	35	2.6	0.1	0.06	0.03
CHE	Ch5.2	877	5	2055	39	3.0	0.1	0.8	0.4
CHE	Ch5.4	114.3	1.2	147	2	0.4	0.1	0.4	0.2
CHE	Ch10b.1	627	3	208	7	1.7	0.1	0.31	0.05
CHE	Ch10b.1	891	7	195	25	1.8	0.1	0.07	0.02
CHE	Ch10b.1	677	3	288	24	2.8	0.2	0.73	0.08
CHE	Ch10b.1	786	5	179	13	2.2	0.1	0.43	0.06
CHE	Ch10b.1	834	4	157	10	1.7	0.1	0.17	0.04
CHE	Ch10b.2	668	3	116	5	0.6	0.1	0.7	0.1
CHE	Ch10b.2	634	4	152	12	0.9	0.1	0.3	0.1
CHE	Ch10b.3	790	7	134	18	2.1	0.1	0.98	0.09
CHE	Ch10b.3	967	7	151	15	2.3	0.1	0.38	0.06
CHE	Ch10b.3	853	7	82	3	2.1	0.2	0.22	0.06
CHE	Ch10b.3	716	6	147	6	2.1	0.2	0.16	0.03
CHAB	QE34.1	5056	57	155	31	3.5	0.1	1.30	0.09
CHAB	QE34.1	5036	44	262	15	3.2	0.1	12.4	0.2
CHAB	QE34.3	7738	109	182	7	4.2	0.2	20.1	0.6
CHAB	QE34.3	3086	71	437	13	3.3	0.1	0.14	0.01
CHAB	QE34.3	208.7	1.3	312	8	4.1	0.1	33.2	0.7
CL	QE6.1	466	3	1970	49	9.8	0.4	13.9	0.2
CL	QE6.1	431	3	2090	29	7.0	0.2	13.7	0.4
<i>Actinolite</i>									
CHE	Ch1.3	183	4	77	7	1.4	0.3	2.24	0.08
CHE	Ch3.2	135	2	31	4	0.6	0.1	0.34	0.02

(continued on next page)

Table 2 (continued)

Massif	Sample	F	2 $\sigma$	Cl	2 $\sigma$	B	2 $\sigma$	Li	2 $\sigma$
<i>Actinolite</i>									
CHE	Ch3.3	132.0	0.9	652	89	2.9	0.3	1.5	0.2
CHE	Ch5.4	36.8	0.3	17.2	1.2	2.0	1.0	7	6
CHAB	QE32.1	54.0	0.3	14.5	0.3	1.4	0.06	4.7	0.07
CHAB	QE32.1	48.7	0.2	132	21	10.4	0.2	58.9	0.5
<i>Epidote</i>									
CHE	Ch3.2	260	10	80.0	1.9	2.51	0.13	1.85	0.28
CL	Cl2.1	4.81	0.17	20.6	0.3	6.13	0.10	23.0	0.2
CL	Cl2.1	8.9	1.4	114	11	3.38	0.07	0.80	0.04
<i>Chlorite</i>									
CHE	Ch3.3	22	66	N.D.	N.D.	2.62	0.07	15.4	0.3
CHE	Ch5.2	44.9	0.2	90	4	5.81	0.07	148.8	1.3
CHE	Ch5.4	32.72	0.15	113	4	4.38	0.11	0.43	0.01
EC	CE8A.2	33.9	0.2	68	2	5.92	0.12	0.24	0.01
EC	CE8A.2	30.78	0.12	29	2	5.88	0.12	0.39	0.02
EC	CE8A.3	35.2	0.3	109	5	7.25	0.13	0.21	0.02
TR	TR11.1	44.7	0.9	593	28	8.88	0.10	185	2
<i>Titanite</i>									
CHE	Ch3.4	1534	3	76	4	0.85	0.06	1.04	0.11
CHE	Ch3.4	933	6	97	8	1.06	0.09	0.75	0.07
CHAB	QE34.1	504	4	58	3	9.14	0.13	6.11	0.07
CHAB	QE34.1	521.2	1.0	29	2	16.9	0.2	0.16	0.01
CHAB	QE34.3	421.5	1.3	38.3	1.2	19.7	0.3	0.23	0.02
CHAB	QE34.3	494.0	1.7	17.9	0.2	23.5	0.2	0.12	0.01
CL	Cl2.1	202.2	1.2	18.6	0.4	7.09	0.13	1.83	0.04
CL	Cl2.1	192.0	0.9	46	3	4.73	0.11	0.39	0.03
CL	Cl2.1	214.3	0.7	59	4	4.38	0.11	0.43	0.01
CL	Cl2.2	288.0	0.6	52	2	5.92	0.12	0.24	0.01
CL	Cl2.2	355.6	1.7	84	5	5.88	0.12	0.39	0.02
CL	Cl2.2	287.3	0.9	24	2	7.25	0.13	0.21	0.02
CL	Cl2.3	251.1	1.1	17.1	0.3	6.9	0.2	0.33	0.03
CL	Cl2.3	215.9	1.6	21.6	1.1	4.48	0.12	0.38	0.02
CL	Q13.2	983	2	64	6	14.1	1.2	16.5	0.5
CL	Q13.2	1210	3	185	7	1.68	0.15	1.19	0.17
CL	Q13.3	871.2	1.9	98	5	3.4	0.2	5.1	0.3
<i>Ilmenite</i>									
CHE	Ch5.1	2.33	0.10	18	2	N.D.	N.D.	N.D.	N.D.
CHE	Ch5.2	1.72	0.11	17.2	1.5	N.D.	N.D.	N.D.	N.D.
CHE	Ch5.4	4.1	0.4	75	4	N.D.	N.D.	N.D.	N.D.
CHE	Ch5.4	4.5	0.3	64	4	N.D.	N.D.	N.D.	N.D.
CHAB	QE34.3	65.1	1.1	103	4	N.D.	N.D.	N.D.	N.D.
CHAB	QE34.1	114.8	0.4	27	3	N.D.	N.D.	N.D.	N.D.
CHAB	QE34.1	222.2	0.9	74	27	N.D.	N.D.	N.D.	N.D.
<i>Glaucophane</i>									
CHAB	QE34.3	51.6	0.9	92	15	5.9	0.1	65.7	0.8
CHAB	QE34.3	57.1	0.7	78	7	6.2	0.1	59.7	1.1
CHAB	QE34.3	79	2	43	9	4.9	0.1	75.3	1.3
CHAB	QE33b.3	54	3	360	101	5.8	0.1	83.4	1.1
CHAB	QE33b.3	44.5	0.4	48	8	6.3	0.1	144.0	1.5
CHAB	QE34.1	48.1	1.0	126	17	5.09	0.09	63.0	0.8
CHAB	QE34.1	40	2	127	45	3.81	0.08	56.0	1.1
CHAB	QE32.2	61	3	213	58	13.3	0.3	136	3
CL	QE6.1	125.3	0.9	31	5	4.2	0.1	67.1	0.5
CL	QE6.1	65.7	0.7	33	3	10.9	0.1	105.8	0.7
CL	QE6.1	100.4	0.5	72	2	17.6	0.3	110.2	1.0
CL	QE6.1	98.5	1.6	46	6	17.9	0.3	113.6	1.3
CL	Cl2.3	34.8	0.4	35.5	1.9	5.4	0.2	180	6
CL	Cl2.3	29.3	0.4	16.9	1.5	9.6	0.2	173	5
CL	Cl2.1	34.7	0.4	24	2	5.4	0.1	152	3
CL	Cl2.1	33.0	0.5	46	3	5.8	0.1	142.7	1.6
CL	Cl2.1	30.2	0.9	98	9	6.7	0.2	105.3	1.9
CL	Cl2.2	50.1	0.2	48	7	8.9	0.2	185	4
CL	Cl2.2	31.2	0.4	59	7	5.8	0.1	149	3
CL	Q13.3	67.9	0.8	109	16	5	1	267	8
CL	Q13.3	70	2	104	20	4.8	0.9	312	6
CL	Q13.3	81	2	198	22	1.8	0.1	247	7
CL	Q13.2	66	2	123	20	4.4	0.2	310	5
CL	Q13.2	71.9	1.2	48	7	2.0	0.2	179	3
EC	CE8A.3	38.0	0.5	34	7	13.4	0.2	332	4
EC	CE8A.3	127.3	1.6	42	3	13.4	0.2	332	4
EC	CE8A.3	30.8	0.3	18	4	14.5	0.2	314	8
EC	CE8A.3	41.8	0.4	23	4	14.5	0.2	314	8
EC	CE8A.3	56.9	0.7	32	4	14.5	0.2	314	8

Table 2 (continued)

Massif	Sample	F	2 $\sigma$	Cl	2 $\sigma$	B	2 $\sigma$	Li	2 $\sigma$
<i>Glaucofane</i>									
EC	CE8A.1	53.3	0.3	22.7	1.8	6.3	0.1	567	6
EC	CE8A.2	76.7	0.9	5.3	0.6	7.8	0.2	375	10
EC	CE8A.2	42.9	1.2	52	8	10.1	0.2	620	9
TR	TR11.1	27	2	108	12	3.8	0.1	110	2
TR	TR11.2	27.8	0.1	64	5	4.8	0.1	112	3
TR	TR11.2	28.4	0.9	42	8	3.9	0.6	77	17
TR	TR16.3	17.4	0.5	42	7	8.1	0.2	119	2
TR	TR16.3	22.0	0.4	59	19	3.1	0.2	108	2
TR	TR16.3	18.1	0.3	86	12	1.7	0.2	82.6	1.5
TR	TR16.2	22.6	0.5	59	9	1.9	0.1	132.6	1.5
TR	TR16.1	23.1	1.6	55	6	2.3	0.2	57	2
TR	TR16.1	24.5	0.5	91	13	1.3	0.1	6.3	0.3
TR	TR16.1	18.8	0.3	57	17	5.4	0.2	81	2
MV	QE29d.3	177	2	59	7	3.5	0.1	12.8	0.2
MV	QE29d.3	190.1	1.8	53	7	3.35	0.07	16.8	0.2
MV	QE29d.3	214.2	1.6	146	51	3.32	0.08	14.3	0.2
MV	QE29d.4	197.6	1.4	43	6	3.6	0.2	21.7	0.5
MV	QE29d.4	157.4	1.9	24.8	1.1	3.8	0.2	18.0	0.3
MV	Gala.1	91.0	1.3	26	3	1.51	0.08	115.4	0.9
MV	Gala.4	121.4	1.7	27	3	2.0	0.2	95.1	0.4
MV	Gala.4	93.9	0.6	32	4	4.7	0.2	100	3
<i>Lawsonite</i>									
CHAB	QE32.1	14.7	1.4	88	8	11.10	0.09	0.39	0.08
CL	QE6.1	50.8	1.1	65	8	9.59	0.14	1.50	0.04
CL	QE6.1	43.8	1.2	69	9	12.91	0.09	0.84	0.01
<i>Rutile</i>									
MV	Gala.1	15.72	0.04	12.0	0.5	N.D.	N.D.	N.D.	N.D.
MV	Gala.4	9.17	0.04	6.12	0.13	N.D.	N.D.	N.D.	N.D.
<i>Omphacite</i>									
MV	Gala.1	12.3	0.4	79	10	2.10	0.04	42.36	0.16
MV	Gala.1	11.4	0.5	127	8	1.20	0.03	71.1	0.3
MV	Gala.1	9.5	0.2	145	7	1.20	0.03	71.1	0.3
MV	QE29d.4	21.9	0.7	97	5	2.40	0.12	22.8	0.4
MV	QE29d.4	12.2	0.3	46.7	1.5	3.68	0.08	21.7	0.3
MV	Gala.4	5.78	0.05	20.8	0.7	1.00	0.03	19.7	0.3
MV	Gala.4	6.48	0.11	200	12	1.86	0.08	51.2	0.3
<i>Garnet</i>									
MV	QE29d.3	8.2	0.3	53	7	0.53	0.03	0.92	0.02
MV	Gala.1	3.89	0.13	64	4	1.09	0.05	1.29	0.03
MV	QE29d.4	18.61	0.13	9.4	0.7	0.65	0.09	0.87	0.04
MV	Gala.4	4.5	0.3	14.9	1.0	0.51	0.08	0.63	0.05
<i>Quartz</i>									
MV	Gala.4	1.3	0.1	30	2	0.85	0.12	0.38	0.03
<i>Phengite</i>									
MV	QE29d.3	428	2	65	5	104.8	0.8	0.95	0.01
MV	QE29d.4	348	3	37.5	0.7	130.6	0.4	1.35	0.03
MV	QE29d.4	305	2	43	3	198.0	0.7	0.99	0.02

CHAB: Chenaillet; TR: Tour Real; CHAB: Chabrière; CL: Clausis; EC: Echassier; MV: Monviso.

interstitial ilmenite (Fig. 2b) show TiO<sub>2</sub> and Al<sub>2</sub>O<sub>3</sub> contents ranging from 34.7 to 43.6 wt% and from 0.2 to 2.9 wt% respectively. Actinolites are associated with Fe-chlorite and epidote. They are characterized by low TiO<sub>2</sub> (<1 wt%) and Al<sub>2</sub>O<sub>3</sub> (<3 wt%) contents relative to amphibole coronas (Fig. 5).

Magmatic clinopyroxenes and ilmenites display low halogens concentrations (F = 2–5 ppm, Cl = 17–68 ppm) relative to amphibole porphyroclasts (F = 1225–2011 ppm, Cl = 28–280 ppm) in Chenaillet metagabbros. This observation is in good agreement with previous studies on Mid-Atlantic Ridge (MAR) metagabbros where magmatic amphibole F and Cl concentrations range from 1000 to 4200 ppm and from 20 to 130 ppm, respectively (Coogan et al., 2001; Cortesogno et al., 2000). Among magmatic minerals, no variations in B or Li concentrations have been observed. The B and Li concentrations of magmatic minerals range from 0.5 to 5 ppm and 0.2 to 2 ppm, respectively. The recrystallization of amphibole porphyroclasts to amphibole corona is accompanied with a decrease of F (90–1970 ppm) and an increase of Cl (80–2060 ppm) and B (0.6–34 ppm) concentrations (Fig. 6a–c). In

contrast, Li (0.4–6 ppm) concentrations remain constant during the recrystallization of amphibole porphyroclasts into amphibole coronas (Fig. 6d). The actinolite–chlorite–epidote assemblages display low F (5–260 ppm) and Cl (17–652 ppm), concentrations relative to amphibole coronas and similar B (1–6 ppm) and Li (0.3–15 ppm) concentrations (Fig. 6a–d). Coronitic titanite surrounding ilmenite displays higher F (933–1534 ppm) and Cl (76–97 ppm) concentrations relative to that of ilmenite.

#### 4.2. Prograde metamorphism in the Queyras and Monviso metagabbros

To constrain the behavior of volatiles during subduction, 8 metagabbros from the Queyras Schistes Lustrés complex (Chabrière, Clausis, Tour Real) and 2 eclogites from the Monviso meta-ophiolite have been analyzed (Table 1). In addition, 2 metasomatic zones in the Echassier and Clausis meta-ophiolites were analyzed to decipher the behavior of volatile during metasedimentary rock/metagabbro interactions.

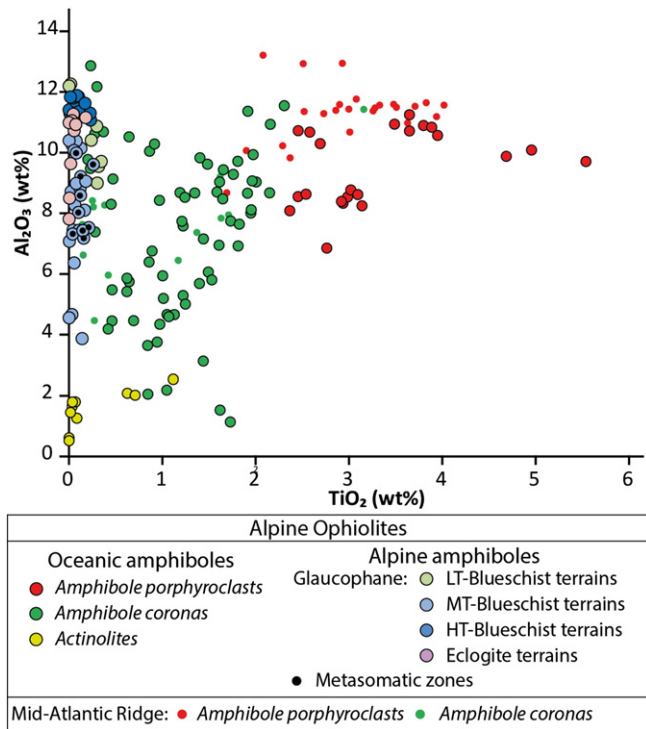


Fig. 5. Plot of amphibole  $\text{Al}_2\text{O}_3$  and  $\text{TiO}_2$  contents.

Queyras metagabbros can preserve relicts of oceanic metamorphism in low metamorphic grade meta-ophiolites (Chabrière and Clausis, Fig. 3a, b). The major element concentrations of oceanic assemblages are similar to that described in Chenaillet metagabbros. Only amphibole porphyroclasts have a wider range of composition ranging from edenite ( $\text{TiO}_2 = 2.8\text{--}5$  wt%;  $\text{Al}_2\text{O}_3 = 7\text{--}10$  wt%) to kaersutite ( $\text{TiO}_2 > 5$  wt%;  $\text{Al}_2\text{O}_3 = 9.7$  wt%). Kaersutites have been observed in one sample (metadiorite–QE32) and are associated with igneous apatites which act as a sink for halogens during magmatic differentiation (Nash, 1976). These amphiboles have abnormally low F ( $= 281\text{--}381$  ppm) and high Cl ( $35\text{--}1224$  ppm) concentrations relative to other magmatic amphibole from alpine or MAR metagabbros (Fig. 6e, f). Other magmatic phases in Queyras metagabbros (ilmenite, clinopyroxene and edenite) are characterized by higher F and Li concentrations relative to the one of Chenaillet metagabbros (Table 2, Fig. 6). However, as previously observed, the recrystallizations of amphibole porphyroclasts ( $F \sim 7120$  ppm;  $\text{Cl} \sim 210$  ppm) into amphibole coronas result in a decrease of F ( $210\text{--}7740$  ppm) and an increase of Cl ( $= 155\text{--}2090$  ppm) concentrations (Fig. 6e, f) whereas no significant changes of B ( $3\text{--}10$  ppm) and Li ( $0.1\text{--}36$  ppm) concentrations are observed (Fig. 6g, h).

The Queyras metagabbros display the progressive recrystallization of oceanic parageneses into blueschist facies assemblages and are composed of glaucophane, lawsonite, albite and epidote ( $^+/-$  actinolite). Glaucophanes display a homogenous major element composition in the different studied ophiolites. They are characterized by low  $\text{TiO}_2$  ( $< 0.3$  wt%) contents relative to LP-amphiboles (Fig. 5) and variables  $\text{Al}_2\text{O}_3$  contents ( $3.9\text{--}12.3$  wt%). Glaucophane has lower F and Cl, and higher Li concentrations relative to LP-amphiboles (Fig. 7). Their volatile concentrations range from 17 to 125 ppm for F, from 17 to 360 ppm for Cl, from 6 to 184 ppm for Li and from 1 to 18 ppm for B. Among the different studied meta-ophiolites, glaucophanes in shear zones (Tour Real) are characterized by the lowest F concentrations (Fig. 7a). Lawsonite and epidote has low F ( $5\text{--}51$  ppm), Li ( $0.4\text{--}23$  ppm) and similar Cl ( $21\text{--}114$  ppm), B ( $3\text{--}13$  ppm) to that of glaucophane (Table 2). In the metasomatic zones, glaucophane and titanite are characterized by high Li concentrations ranging from 180 to 620 ppm (Fig. 7c, Table 2).

The eclogitic paragenesis of Monviso metagabbros is composed of glaucophane, garnet, omphacite, quartz and rutile. Glaucophane from the Monviso meta-ophiolite displays low  $\text{TiO}_2$  contents ( $< 0.2$  wt%) and a wide range of  $\text{Al}_2\text{O}_3$  contents ( $= 7.8\text{--}11.3$  wt%) overlapping the compositions of glaucophane from blueschist terrains (Fig. 5). Garnets display a mixed composition between almandine and grossular end-members with low pyrope content (Table C1). Glaucophane from Monviso meta-ophiolite is characterized by higher F and similar Cl, Li and B concentrations relative to glaucophane from blueschist terrains (Fig. 7). Their volatile concentrations range from 91 to 214 ppm for F, from 25 to 146 ppm for Cl, from 14 to 115 ppm for Li and from 1 to 5 ppm for B. Omphacite has low F ( $6\text{--}22$  ppm) and similar Cl ( $21\text{--}200$  ppm), Li ( $20\text{--}71$  ppm) and B ( $1\text{--}4$  ppm) concentrations relative to glaucophane. Garnet ( $F = 4\text{--}19$  ppm;  $\text{Cl} = 9\text{--}64$  ppm;  $\text{Li} = 0.6\text{--}1.3$  ppm;  $\text{B} = 0.5\text{--}1.1$  ppm) and rutile ( $F = 9\text{--}16$  ppm;  $\text{Cl} = 6\text{--}12$  ppm) has low volatile concentrations relative to other eclogitic minerals.

## 5. Discussion

During oceanic and subduction metamorphism, the different phase transitions of amphiboles are accompanied with variations in F, Cl, Li and B concentrations (Figs. 6 and 7) suggesting that these elements are mobile in fluids on a large scale. In order to better constrain the fate of F, Cl, Li and B, we adapted a method combining the in situ F, Cl, Li and B measurements of the minerals with their respective estimated modal proportions to calculate the bulk volatile composition (Appendix C, Table C3 and Fig. 8). This reconstitution of bulk composition by mineral paragenesis was expected to track the evolution of bulk budget of F, Cl, Li and B in metagabbros from their crystallization and hydration at the ridge to their devolatilization in subduction zones and thus to give insight into gains or losses during fluid/rock interactions. Indeed, the fate of volatile elements in metagabbros during subduction is difficult to evaluate with direct bulk rock measurements since prograde metamorphism leads to the progressive, but incomplete, recrystallization of LP-paragenesis into HP-paragenesis (Fig. 3). Furthermore, these rocks can also partly record a late metamorphism during massif exhumation (Fig. 3b). Bulk rock measurements of volatile elements integrate all these metamorphic processes and are thus not representative of different recrystallization stages of metagabbro during subduction. It is important to note that few studied metagabbros contain igneous apatites (Table 1) which can incorporate high halogens concentrations (up to several wt%, e.g. Nash, 1976). However, this mineral is poorly affected by prograde metamorphism in metagabbros. Indeed, experimental studies have shown that this mineral is stable up to 7.5 GPa and 950 °C in a typical eclogite assemblage (Konzett and Frost, 2009). Furthermore, it should be noted that apatite abundance in an altered oceanic gabbros is about 0.1 wt% (based on  $\text{P}_2\text{O}_5 = 0.04$  wt%, Hart et al., 1999), which is low relative to amphibole abundance in these rocks ( $> 10$  wt%). Therefore apatite breakdown does not greatly affect halogen transfers between the slab and the source of arc magmas in subduction zones and have not been considered in the bulk composition reconstitution.

### 5.1. The oceanic crust before its subduction

To characterize fluid and chemical exchanges in subduction zones, it is crucial to determine the composition of the material that enters in the subduction zone. The Ligurian oceanic lithosphere is characterized by a heterogeneous crust (metabasalts and metagabbros) associated with serpentinites and metasedimentary rocks of various origin (Bernoulli et al., 2003; Lagabrielle et al., 2014; Manatschal et al., 2011; Tricart and Lemoine, 1986). The volatile concentrations of these three different reservoirs are summarized in Table 3. Relative to other lithologies, metagabbros can integrate a significant amount of halogens and thus play an important role in these elements cycle in subduction zones. At

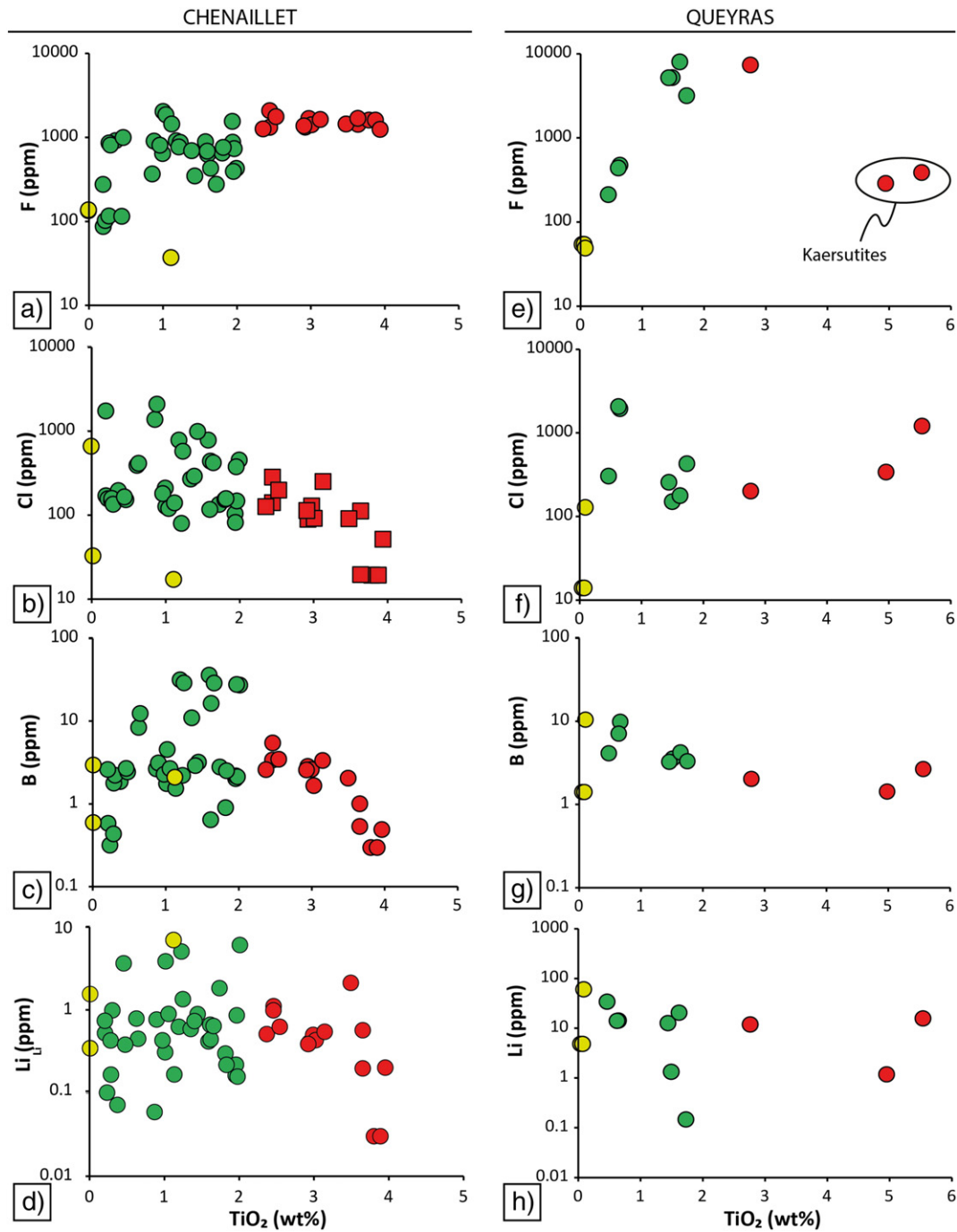


**Fig. 6.** Plots of  $\text{TiO}_2$  vs F, Cl, Li and B concentrations of LP-amphiboles in Chenailet metagabbros (a–d) and LP-amphiboles relic in Queyras Schistes Lustres metagabbros (e–h). Symbol captions: see Fig. 5. These figures show the compositional evolution of amphibole during oceanic lithosphere cooling and seafloor metamorphism.

the opposite, metagabbros B and Li concentrations are low compared to other lithologies (Table 3).

During oceanic spreading, the igneous crust is continuously modified by the percolation of fluids. This process leads to the crystallization of several generations of amphiboles (amphibole porphyroclasts, amphibole coronas and actinolites), of which the pressure and temperature of crystallization can be assessed by the Ca-amphibole thermobarometer of Ernst and Liu (1998). The Ernst and Liu (1998) thermometer is based on the  $\text{TiO}_2$  content of amphiboles and requires an excess of Ti in the system, such conditions are met when Ti is present as an oxide (ilmenite, rutile) or in titanite. The accuracy of the thermometer has been estimated at the Institut für Mineralogie (Hannover, Germany) using published and unpublished experimental data, and temperature estimates are accurate

to  $\pm 40^\circ\text{C}$  (J. Koepke, pers. comm.). The equilibration temperature of Ca-amphiboles progressively decreases from amphibole porphyroclasts to amphibole coronas. The amphibole porphyroclasts display near solidus magmatic temperature ranging from  $1000^\circ\text{C}$  to  $880^\circ\text{C}$  whereas temperature equilibration of amphibole coronas ranges from  $830^\circ\text{C}$  in light brown amphiboles to  $520^\circ\text{C}$  in green amphiboles. Amphibole porphyroclasts record pressures less than 0.5 GPa, which is in agreement with the emplacement of the gabbros at LP in the oceanic lithosphere. Ernst and Liu (1998) predict a decrease of  $\text{Al}_2\text{O}_3$  contents in amphiboles during the isobaric cooling of metagabbros. However, amphibole coronas display a wide range of  $\text{Al}_2\text{O}_3$  contents that correspond to unrealistic pressure equilibrations ranging from negative values to 1.7 GPa. Indeed, amphibole coronas can exsolve  $\text{TiO}_2$  as titanite (Fig. 2b),

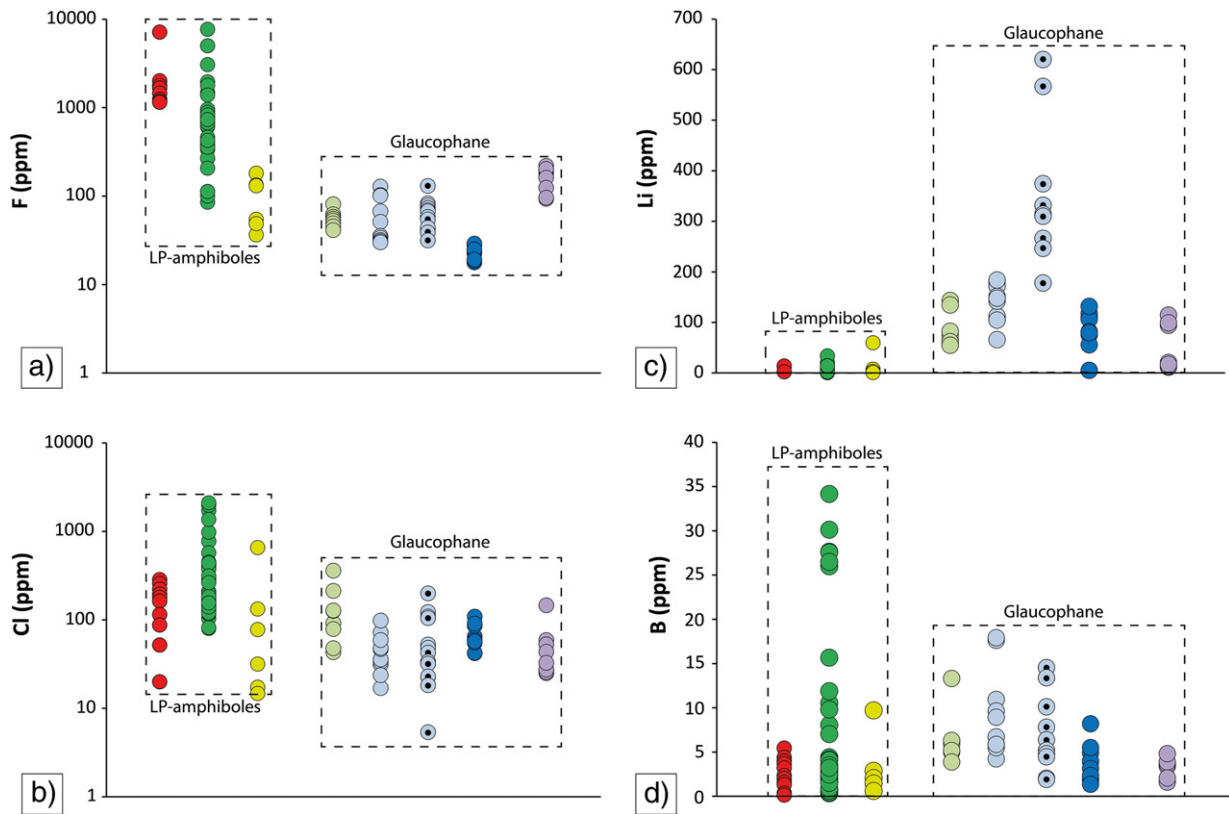


**Fig. 7.** Plots of F, Cl, Li and B concentrations of amphiboles from greenschist to eclogitic facies metagabbros indicating the change of volatile element concentrations with glaucophane crystallization. Symbol caption: see Fig. 5.

whereas there is no evidence of  $\text{Al}_2\text{O}_3$  redistribution during oceanic lithosphere cooling explaining these unrealistic pressure estimates (Debret et al., 2013a; Ernst and Liu, 1998). The actinolite–chlorite–epidote paragenesis is typical from low temperature greenschist facies conditions (e.g. Spear, 1993). It represents the last stages of metamorphism recorded by ophiolitic metagabbros before subduction and/or during massif exhumation/obduction.

LP-amphiboles and titanites have the highest F and/or Cl concentrations of all the mineral phases in metagabbros and are significant carrier of halogens in these rocks (Fig. 8). Ultimately it is the fate of these phases that control the F–Cl budget of the crust during its cooling and hydration in oceanic setting. Amphibole porphyroclasts display higher F and similar Cl concentrations relative to other magmatic phases (Fig. 9a). The calculated bulk rock composition shows that amphibole porphyroclasts crystallization could be accompanied with an increase of F concentrations (300–650 ppm) relative to MORB composition (11–100 ppm). Such high F concentrations can be explained by the addition of F during melt crystallization (e.g. assimilation of previously hydrothermally altered crust; France et al., 2013) and/or by the release of an F-depleted component during fractional crystallization (Coogan et al., 2001). Amphibole coronas display a wide range of F concentrations overlapping that of amphibole porphyroclasts (Figs. 6a–e and 8a). However, in the same rock, F concentrations systematically decrease by a factor of 2 to 10 during amphibole porphyroclasts recrystallization into amphibole corona (see samples Ch 3.3, 3.5, 5.1, 5.2, and 5.4; Ch 3.1 is an exception, Table 2). This apparent decrease of F abundance during lithosphere cooling can be explained by (i) a redistribution of F between F-rich titanite and amphibole coronas during amphibole porphyroclasts recrystallization or (ii) a leaching of F by fluids. The calculated bulk rock composition ranges from 200 to 500 ppm, which is similar to previous estimates (300 to 650 ppm, Fig. 8), suggesting that F leaching in metagabbros during seafloor metamorphism is minimal. Chlorine concentrations in amphibole coronas are systematically higher than those of magmatic phases. Furthermore,

bulk rock reconstitution show that the crystallization of amphibole coronas is accompanied with an increase of metagabbros Cl concentrations (Fig. 8). Given high Cl concentration in seawater, the high concentration of amphibole coronas are usually interpreted as resulting of seawater/rock interaction during lithosphere cooling and hydration (e.g. Coogan et al., 2001; Vanko, 1986). Actinolite, epidote and chlorite greenschist paragenesis has low F and Cl concentrations relative to amphibole porphyroclasts or amphibole corona (Fig. 9a).

Li and B concentrations of calculated bulk rocks are relatively constant throughout oceanic crust cooling and hydration. The Li concentrations of amphibole coronas overlap that of magmatic minerals or MORB (Fig. 9b) suggesting that Li is immobile during HT oceanic metamorphism. The Li concentrations of amphibole coronas are thus assumed to be inherited from magmatic minerals (clinopyroxene, plagioclase or amphibole porphyroclasts). In the Chenaillet massif, few analyses of epidote and chlorite display higher Li concentrations relative to amphibole porphyroclasts or amphibole coronas (Table 2, Fig. 9b). However, we did not detect significant Li addition in the bulk calculation. Such enrichments can thus be interpreted as localized late fluid circulations occurring in an open system during massif oceanization, subduction or obduction (see discussion below). The B concentrations of metamorphic minerals formed during oceanic lithosphere hydration are commonly attributed to seafloor derived fluids (Coogan et al., 2001; Gillis et al., 2003; Vils et al., 2008). Nevertheless, the studied metagabbros show little evidence of a B concentration increase during hydrothermal alteration since amphibole coronas, titanite, actinolite, epidote or chlorite display roughly similar B concentrations relative to magmatic minerals (Fig. 9b) and there is no correlation between B and Cl abundance in amphibole.

### 5.2. Fate of volatile elements in the slab during amphibole breakdown

Amphibole porphyroclasts, amphibole coronas and titanites have the highest F and Cl concentrations relative to others magmatic or

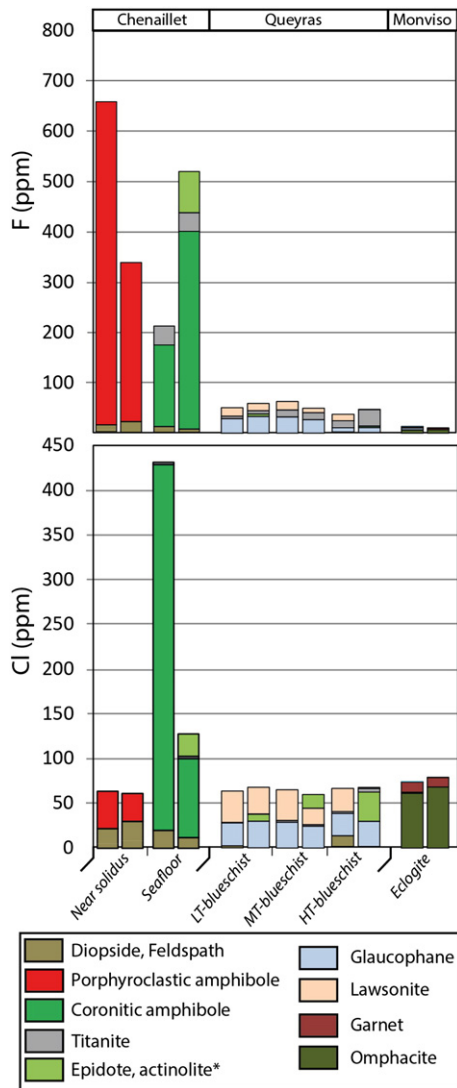


**Fig. 8.** Reconstitution of bulk rock composition (corresponding samples, from left to right: Ch3, Ch5, QE34, QE32, QE9, Cl2, TR11, TR16, QE29, Gala) showing a sharp decrease of halogen concentrations passing from Chenaillet to Queyras or Monviso metagabbros. \*Epidote and actinolite crystallization can be related to late seafloor or obduction/exhumation metamorphism.

metamorphic phases composing oceanic metagabbros (Fig. 9a). The breakdown of these phases is thus critical to constrain halogens fluxes between the slab and the mantle wedge in subduction zones. In the following discussion, the Queyras Schistes Lustrés complex, a metasedimentary-rich environment interpreted as a paleo-sedimentary wedge (Tricart and Schwartz, 2006), and the Monviso meta-ophiolite, a remnant of the oceanic lithosphere preserving a large portions of the oceanic crust (Angiboust et al., 2011), are discussed separately since in both settings the nature of fluid/rock interaction are different (Lafay et al., 2013).

### 5.3. Metasedimentary rock/metagabbros fluid interactions in the Queyras ophiolites

In the Queyras metagabbros, titanite inclusions remain unaffected during amphibole coronas recrystallization into glaucophane (Fig. 3b) suggesting that this mineral is stable at these P-T conditions. The recrystallization of oceanic assemblages at blueschist facies P-T conditions can

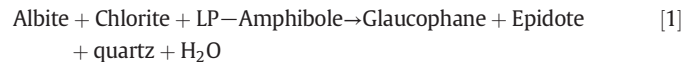
**Table 3**

Volatile (F, Cl, B and Li) contents of lithosphere reservoirs during oceanic and subduction metamorphism.

Lithologies	F (ppm)	Cl (ppm)	B (ppm)	Li (ppm)	ref.
<i>Oceanic lithospheric budget</i>					
Serpentinities	50–520*	260–7100	10.4–65	0.1–3.4	1,2,3,4,5
Sediments	400–1300	21–2000	100–230	5.4–74	6,7,8,9
MORB	11–100	6–50	0.5	5.4–6.9	10,11
AOC	160–216	79–1432	0.2–6	9–33	12,13,14
Chenaillet/Chabrière metagabbros	42–657 (317†)	38–425 (123†)	0.6–1.9 (1.4†)	0.3–2.3 (1.8†)	
<i>Western Alps subduction</i>					
Queyras serpentinites	–	–	30–174*	0.1–4	15
Queyras metasedimentary rocks	–	–	32–374	10–127	15, 16
Queyras metagabbros	27–62 (50†)	57–68 (63†)	4–24 (10†)	29–140 (62†)	
Queyras metasomatic zones	57	131	13	143	
Monviso metagabbros	10–16 (13†)	71–79 (75†)	1–4 (3†)	9–34 (20†)	
Monviso serpentinites	3.6–11.3*	20–246*	10–11*	0.2	1, 15

1 Debret et al., 2014; 2 Orberger et al., 1999; 3 Bonifacie et al., 2008; 4 Vils et al., 2008; 5 Barnes and Sharp, 2006; 6 Li, 1982; 7 Li, 1991; 8 John et al., 2011; 9 Bouman et al., 2004; 10 Hart et al., 1999; 11 Salters and Stracke, 2004; 12 Wedepohl and Hartmann, 1994; 13 Straub and Layne, 2003; 14 Sano et al., 2008; 15 Lafay et al., 2013; 16 Bebout et al., 2013; \*in situ measurements; † mean value.

thus be summarized in a relatively closed system by the following general and unbalanced reactions:



A second possibility to consider is the effect of fluid infiltration/percolation during recrystallization at blueschist facies (e.g. Ballèvre et al., 2003). The interaction between external fluids and the surrounding lithologies at high pressure results in significant enrichment in fluid mobile elements (Lafay et al., 2013; Marschall et al., 2009; Penniston-Dorland et al., 2012; Vitale Brovarone et al., 2014).

The Queyras Schistes Lustrés complex is considered as an open system where fluids released during sediment dehydration has infiltrated the surrounding rocks during subduction (Lafay et al., 2013; Schwartz et al., 2013). Metasomatic contacts between metagabbros and metasedimentary rocks (Fig. 3c) or glaucophane bearing shear zones in metagabbros embedded in serpentinites (Fig. 3e) provide evidence of fluid/rock interaction between these different lithologies during subduction. The calculated bulk rock compositions of Queyras metagabbros show that these rocks display high Li concentrations relative to oceanic metagabbros. Such increase of Li in alpine metamorphic rocks has been reported previously and interpreted as retrograde metamorphic processes (Marschall et al., 2007, 2009; Zack et al., 2003) due to a stronger affinity of Li to silicate mineral over aqueous fluids at temperature lower than 250 °C (Berger et al., 1988; Marschall et al., 2007). However, in the studied metagabbros, glaucophane is the main carrier of Li in blueschist metagabbros (Fig. 9). This mineral often replaces LP amphiboles (Fig. 3a, b) and sometimes show euhedral shapes (Fig. 3d) suggesting that it has crystallized at HP during prograde metamorphism and is poorly affected by retrograde metamorphic reactions. Glaucophane displays higher Li concentrations relative to oceanic assemblages, reaching up to 620 ppm in metasomatic zones. We thus propose that Li has been mobilized from surrounding sediments during the first stage of prograde metamorphism, at temperature above 250 °C. These Li-rich fluids could have promoted glaucophane crystallization. Several studies have underlined similar Li enrichments during prograde metamorphism in meta-ophiolitic environments dominated by metasedimentary rocks

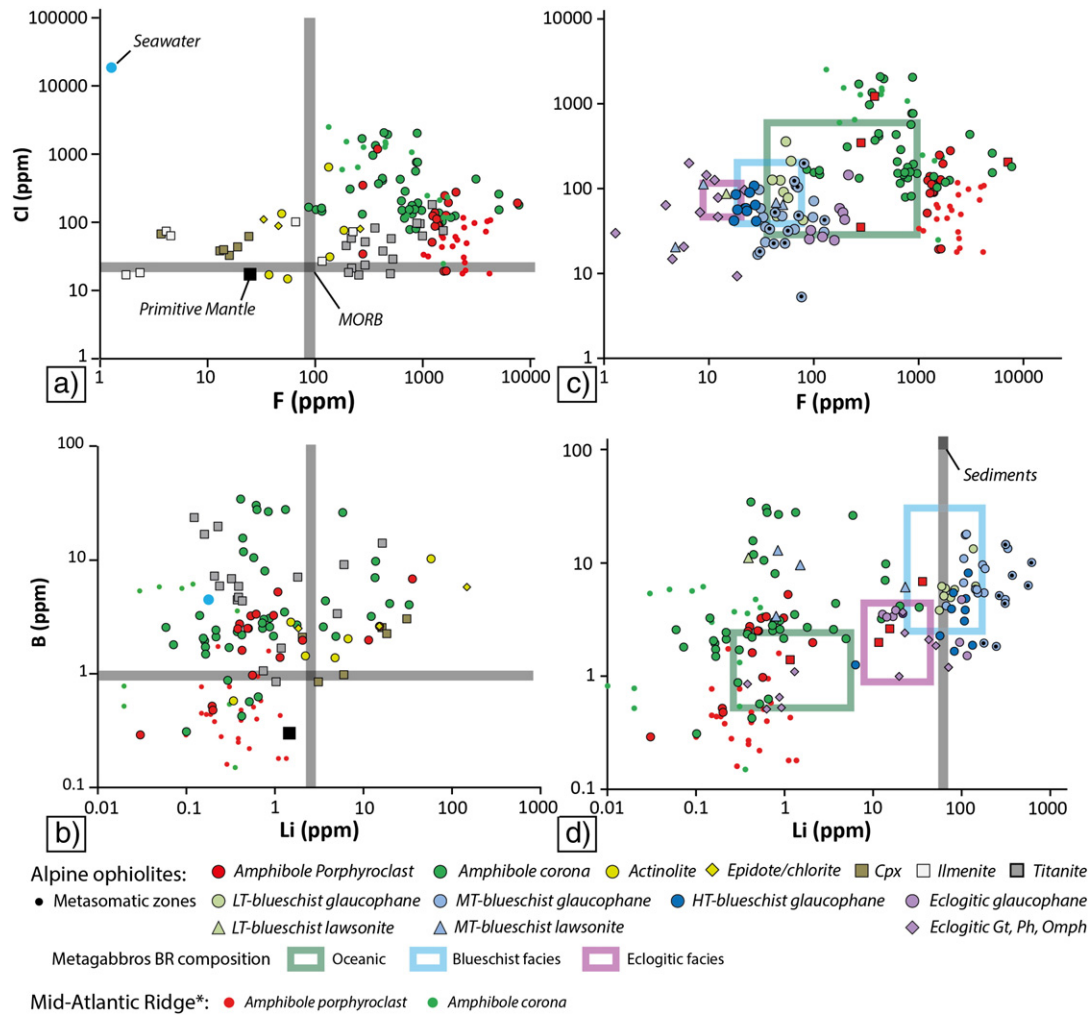


**Fig. 9.** Plots of Cl versus F and B versus Li of (a–b) oceanic (magmatic and metamorphic) assemblages and (c–d) alpine assemblages composing the metagabbros. The seawater value is from Li (1991), the primitive mantle value is from McDonough and Sun (1995) and the MORB value is an average value from Shaw et al. (2010) and Koga (unpublished data, see appendix of Van den Bleeken and Koga, 2015). The sediment value is from Li (1991). \*Values are from Cortesogno et al. (2000) and Coogan et al. (2001); \*\*see discussion and Appendix C for more details.

(e.g. Catalina Schist California, United-States; Penniston-Dorland et al., 2012 or Almiraz massif, Spain; Scambelluri et al., 2004a) suggesting that Li can act as a tracer of element influx from metasedimentary rocks during subduction.

Metasedimentary rocks constitute a huge reservoir of B and Li in the oceanic lithosphere before subduction (Table 3). Previous whole rock and in situ studies of the Queyras Schiste Lustrés complex have shown that B can be mobile in the fluids released during meta-sediments dehydration whereas Li shows an overall retention behavior (Bebout et al., 2007, 2013; Busigny et al., 2003; Garofalo, 2012). However, our study presents high Li concentrations in glaucophane and titanite composing metasomatic contacts between metasedimentary rocks and metagabbros relative to glaucophane and titanite from metagabbroic pods (Fig. 7). This suggests that Li can be mobilized in metasedimentary rock derived fluids but this loss insignificantly affects the bulk Li concentrations of metasedimentary rocks (e.g. Penniston-Dorland et al., 2012). On the contrary, no B enrichment has been observed in the minerals composing these contacts as well as in metagabbroic pods. The sole consideration of metagabbros and metasedimentary rocks inter-exchanges is thus inadequate to explain the mass balance of volatile elements in this system. Notably, metagabbroic pods from the Queyras Schist Lustrés complex are also associated with B-rich antigorite schists (Lafay et al., 2013). In this setting, serpentinites are considered to act as sponges and buffer most of fluid mobile elements released during

metasedimentary rocks dehydration. However, although Li can be easily stored in chrysothile (up to ~ 100 ppm; Lafay et al., 2013; Vils et al., 2010; Wunder et al., 2010), this element is not easily incorporated at HP in antigorite (less than 10 ppm; Debret et al., 2013b; Lafay et al., 2013; Scambelluri et al., 2004a; Vils et al., 2010; Wunder et al., 2010). Antigorite schists therefore serve as poor sinks for Li. This explains the lack of B enrichment and the significant Li enrichment at the greenschist to blueschist transition in metagabbros. This suggests a partitioning of fluid mobile elements among meta-ophiolite lithologies (metagabbros, serpentinites, and metasedimentary rocks) during subduction. During subduction, in an open system where fluid mobile elements are supplied by the dehydration of metasedimentary rocks, lizardite recrystallization into antigorite acts as a sink for B, while Li is mostly incorporated into glaucophane.

In the Queyras metagabbros, no correlation between Li and halogen concentration in glaucophane has been observed suggesting that halogens are poorly affected by fluid/rock interaction during metasedimentary rocks dehydration. The glaucophane and lawsonite/epidote displays similar halogen concentrations, which are lower than those of LP-amphiboles (Fig. 9) whereas quartz contains only traces of halogens (Table 2). These observations are in agreement with F and Cl released by fluids during the recrystallization of amphibole porphyroclasts and amphibole coronas into glaucophane and lawsonite/epidote during subduction. According to previous studies (Debret et al., 2014; Scambelluri

et al., 2004a,b), this suggests that halogens are released in slab-derived fluids during the first stages of subduction.

#### 5.4. Amphibole breakdown in the oceanic crust approaching eclogite facies: the Monviso ophiolite

The eclogitic metagabbros of the Monviso ophiolite are mostly composed of garnet, omphacite, quartz, glaucophane, rutile and phengite. Relative to blueschist metagabbros, they are characterized by a lower modal amount of glaucophane and the disappearance of chlorite, titanite, lawsonite and/or epidote (Tables 1 and A1). Mass balance calculation show that F and Cl abundances of eclogitic metagabbros are lower than that of oceanic metagabbros (Fig. 9; Table 3) suggesting that about 90% and 50% of the initial budget of F and Cl in metagabbros is lost in fluids during the first 80 km of subduction. This observation is in good agreement with the disappearance of oceanic halogen rich phases in eclogitic metagabbros. It suggests that LP-amphiboles and titanite stabilities control the halogens fluxes between the metagabbros and the surrounding environment up to eclogite facies. At greater depth, the fate of halogens can be controlled by omphacite, garnet, phengite and/or glaucophane which are the main carriers of F and Cl in eclogitic metagabbros (Table 2). Phengite is rare in the studied metagabbros and its modal amount is less than 5%. Its crystallization at HP is dependent on the amount of K<sub>2</sub>O in the bulk composition (Poli and Schmidt, 1995) which is expected to be low. Phengite cannot be considered as a significant carrier of F in the studied metagabbros. Glaucophane represent about 5%–10% of the rock and its concentration reaches up to 210 ppm of F in eclogite metagabbros. At eclogite facies, the continuous reactions taking place in metagabbros progressively consume glaucophane and change its composition (Spear, 1993; Poli and Schmidt, 2002). F-abundances in glaucophane increase in eclogitic metagabbros relative to that of Queyras metagabbros. Indeed, the incorporation of fluorine in glaucophane can stabilize it at high temperature and pressure (e.g. Holloway and Ford, 1975), in equilibrium with eclogitic paragenesis (Fig. 4). At greater depth, the glaucophane terminal breakdown can release a significant amount of halogens in fluids. However, it should be noted that other minerals with OH-sites (humites, chlorite or micas) or apatite are all potential F hosts (e.g. Koga et al., 2014) in the subducting slab that can persist to higher pressure and temperature conditions. It is thus plausible to expect that some F persist deeper in subduction zone.

As in the Queyras Schistes Lustrés complex, bulk rock Li abundances, estimated by mass balance calculation, increase passing from oceanic to

eclogitic metagabbros (Table C3) suggesting that Li is added to metagabbros by fluid during subduction. However, in the Monviso massif, the scarcity of metasedimentary rocks, which represent less than 10% of the massif (Schwartz et al., 2001), suggests that fluid/rock interactions between metasedimentary rocks and metagabbros are limited (e.g. Lafay et al., 2013). In contrast, the Monviso is composed of metagabbroic pods embedded into serpentinites. In this massif, previous studies report strong interactions between these two lithologies (e.g. Angiboust et al., 2014). Considering that lizardite breakdown can release a significant amount Li in fluids (Debret et al., 2013b; Vils et al., 2010), the observed Li concentrations of metagabbros can reflect such serpentinites/metagabbros fluid interactions during subduction. B abundances of eclogitic metagabbros and minerals are comparable to oceanic ones (Fig. 9) suggesting that this element is immobile in metagabbros throughout prograde metamorphism in subduction zones.

## 6. Summary

Ligurian ophiolites correspond to the sampling of different levels the oceanic lithosphere. The Chenaillet ophiolite corresponds to a large segment of the Ligurian oceanic crust associated with serpentinites and topped locally by rare metasedimentary rocks. The Queyras meta-ophiolites consist of serpentinites and/or metagabbros that can be associated with their oceanic paleobasement, including opicalcites, pillowed metabasalts and pillow-metabreccias (Lagabrielle et al., 2014). These ophiolites are embedded in a sedimentary rich environment interpreted as a fossiliferous sedimentary wedge (Tricart and Schwartz, 2006). In both settings, the metagabbros are composed of several generations of magmatic and metamorphic amphiboles (Figs. 2, 3a, b) and titanite which store a significant amount of halogens. In contrast, metagabbros store a small amount of B and Li relative to sediments or serpentinites during oceanic spreading (Table 3).

Prior to subduction, amphibole porphyroclast, amphibole corona and titanites constitute the main halogen-bearing phases in metagabbros. It is thus the stability of these phases that governs the flux of halogens between the subducted altered oceanic crust and the mantle wedge in subduction zones. During subduction, the different part of the lithosphere experienced different fluid/rock interactions (Fig. 10). In the Queyras Schistes Lustrés complex, the heavy deformation and the abundant devolatilization of metasedimentary rocks produce large fluid flows that promote rock hybridization at metasedimentary rock/metagabbros (Fig. 3c) or serpentinite contacts. Such mixing zones are likely to exist along the slab-mantle interface

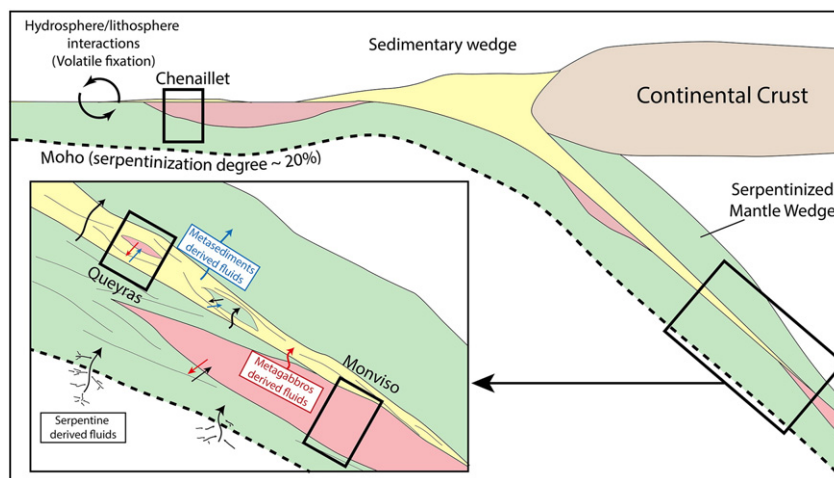


**Fig. 10.** Schematic view of a subduction zone with possible fluid migration pathways based on alpine meta-ophiolite observations. In the down part of the slab, below the Moho, the deformation is limited and volatiles (F, Cl, Li and B) are transported through channelized fluid flows (see Debret et al., 2013b). In the upper part of the lithosphere, the deformation allows a large scale fluid circulation. In metagabbros, the continuous reactions of amphibole disappearance lead to the release of halogens (F and Cl) in fluids while Li can be locally stored in glaucophane and phengite during serpentinites/metagabbros fluid interactions. Above the slab, sediment dehydration releases a large quantity of volatiles that can be transferred to serpentinites and metagabbros boudins and to the mantle wedge.

(e.g. *Bebout, 2014; Konrad-Schmolke et al., 2011*) and act as a filter for geochemical fluxes in subduction zones. In the present study, metagabbro and serpentinite olistoliths can fix some of the Li and B released during metasedimentary rock dehydration and, probably, transport them to greater depth. In contrast, F and Cl are continuously released to fluids and can be transferred at these depths to mantle wedge where halogen-rich fluids can promote the serpentinization of the mantle wedge (e.g. *Guillot et al., 2000*). The Monviso meta-ophiolite preserves a large segment of the oceanic crust (*Angiboust et al., 2011*). The presence of pillow-lavas (*Schwartz et al., 2001*) indicates that this meta-ophiolite correspond to a sampling of the upper part of the slab, probably located just below the slab-mantle interface (*Fig. 10*). In this setting, the interaction with the sedimentary original cover is limited and most of volatile escaped the system. Local enrichment in Li suggests fluid/rock interactions between serpentinites and metagabbros. Such interactions can be linked to local fluid/rock interactions or mark the percolation of deep fluid released by serpentinite dehydration composing the deepest part of the slab (e.g. *Debret et al., 2013b*).

### Acknowledgment

This research was financed by the French Government Laboratory of Excellence initiative no. ANR-10-LABX-0006, the Région Auvergne and the European Regional Development Fund. This is Laboratory of Excellence ClerVolc contribution no. 183. This work was supported by ANR SlabFlux, ANR09BLAN033, CNRS-INSU and by INSU Systerre funding attributed to LMV UMR 6524. The first author is supported by the ERC HabitablePlanet (306655), grant attributed to Helen Williams (Durham University, UK). We thank E. Inglis (Durham University, UK) for its correction of the English in this paper. We thank S. Penniston-Dorlan and an anonymous reviewer for critical comments on earlier version of this article and careful editorial handling by M. Scambelluri.

### Appendix A. Supplementary data

Supplementary data to this article can be found online at <http://dx.doi.org/10.1016/j.lithos.2015.12.004>.

### References

- Agard, P., Vidal, P., Goffé, B., 2001. Interlayer and Si content of phengite in HP-LT carpholite-bearing metapelites. *Journal of Metamorphic Geology* 19, 479–495.
- Anselmi, B., Mellini, M., Viti, C., 2000. Chlorine in the Elba, Monti Livornesi and Murlo serpentines: evidence for sea-water interaction. *European Journal of Mineralogy* 12, 137–146.
- Angiboust, S., Agard, P., Raimbourg, H., Yamato, P., Huet, B., 2011. Subduction interface processes recorded by eclogite-facies shear zones (Monviso, W. Alps). *Lithos* 127, 222–238.
- Angiboust, S., Pettke, T., De Hoog, C.J., Caron, B., Oncken, O., 2014. Channelized fluid flow and eclogite-facies metasomatism along the subduction shear zone. *Journal of Petrology* 55, 883–916.
- Ballèvre, M., Lagabriele, Y., Merle, O., 1990. Tertiary ductile normal faulting as a consequence of lithospheric stacking in the western Alps. *Société Géologique de France, Mémoires* 156, 227–236.
- Ballèvre, M., Pitra, P., Bohn, M., 2003. Lawsonite growth in the epidote blueschists from the Ile de Groix (Armorican Massif, France): a potential geobarometer. *Journal of Metamorphic Geology* 21, 723–735.
- Barnes, J.D., Sharp, Z.D., 2006. A chlorine isotope study of DSDP/ODP serpentinitized ultramafic rocks: Insights into the serpentinization process. *Chemical Geology* 228, 246–265.
- Bebout, G.E., Bebout, A.E., Graham, C.M., 2007. Cycling of B, Li, and LILE (K, Cs, Rb, Ba, Sr) into subduction zones: SIMS evidence from micas in high-P/T metasedimentary rocks. *Chemical Geology* 239, 284–304.
- Bebout, G.E., Agard, P., Kobayashi, K., Moriguti, T., Nakamura, E., 2013. Devolatilization history and trace element mobility in deeply subducted sedimentary rocks: evidence from Western Alps HP/UHP suites. *Chemical Geology* 342, 1–20.
- Bebout, G.E., 2014. Chemical and isotopic cycling in subduction zones. In: Holland, H.D., Turekian, K.K. (Eds.), *Treatise on Geochemistry*, 2nd edition Vol. 4. Elsevier, Oxford, pp. 703–747.
- Berger, G., Schott, J., Guy, C., 1988. Behaviour of Li, Rb and Cs during basalt glass and olivine dissolution and chlorite, smectite and zeolite precipitation from seawater: experimental investigations and modelization between 50 °C and 300 °C. *Chemical Geology* 71, 297–312.
- Bernoulli, D., Manatschal, G., Desmurs, L., Müntener, O., 2003. Where did Gustav Steinmann see the trinity? Back to the roots of an Alpine ophiolite concept. In: Dilek, Y., Newcom, S. (Eds.), *Ophiolite concept and the evolution of geological thought: Boulder, Colorado. Geol. Soc. of America Special Paper* 373, pp. 93–110.
- Bonifacie, M., Busigny, V., Mével, C., Philippot, P., Agrinier, P., Jendrzewski, N., Scambelluri, M., Javoy, M., 2008. Chlorine isotopic composition in seafloor serpentinites and high-pressure metaperidotites. Insights into oceanic serpentinization and subduction processes. *Geochimica et Cosmochimica Acta* 72, 126–139.
- Bouilhol, P., Burg, J.P., Bodinier, J.L., Schmidt, M., Dawood, H., Hussain, S., 2009. Magma and fluid percolation in arc to forearc mantle: evidence from Sapat (Kohistan, Northern Pakistan). *Lithos* 107, 17–37.
- Bouman, C., Elliott, T., Vroon, P.Z., 2004. Lithium inputs to subduction zones. *Chemical Geology* 212, 59–79.
- Busigny, V., Cartigny, P., Philippot, P., Ader, M., Javoy, M., 2003. Massive recycling of nitrogen and other fluid-mobile elements (K, Rb, Cs, H) in a cold slab environment: evidence from HP to UHP oceanic metasediments of the Schistes Lustrés nappe (western Alps, Europe). *Earth and Planetary Science Letters* 215, 27–42.
- Caby, R., 1995. Plastic deformation of gabbros in a slow-spreading mesozoic ridge: example of the Montgenèvre ophiolite, Western Alps. Kluwer academic publishers, pp. 123–145 (Printed in the Netherlands).
- Coogan, L.A., Wilson, R.N., Gillis, K.M., MacLeod, C.J., 2001. Near-solidus evolution of oceanic gabbros: insights from amphibole geochemistry. *Geochimica et Cosmochimica Acta* 65, 4339–4357.
- Cortesogno, L., Gaggero, L., Zanetti, A., 2000. Rare earth and trace elements in igneous and high-temperature metamorphic minerals of oceanic gabbros (MARK area, Mid-Atlantic Ridge). *Contributions to Mineralogy and Petrology* 139, 373–393.
- Dalou, C., Koga, K.T., Shimizu, N., Boulon, J., Devidal, J.L., 2012. Experimental determination of F and Cl partitioning between lherzolite and basaltic melt. *Contributions to Mineralogy and Petrology* 163, 591–609.
- Debret, B., Nicollet, C., Andreani, M., Schwartz, S., Godard, M., 2013a. Three steps of serpentinization in an eclogitized oceanic serpentinization front (Lanzo Massif–Western Alps). *Journal of Metamorphic Geology* 31, 165–186.
- Debret, B., Andreani, M., Godard, M., Nicollet, C., Schwartz, S., 2013b. Trace element behavior during serpentinization/deserpentinization of an eclogitized oceanic lithosphere: a LA-ICPMS study of the Lanzo ultramafic massif (Western Alps). *Chemical Geology* 357, 117–133.
- Debret, B., Koga, K.T., Nicollet, C., Andreani, M., Schwartz, S., 2014. F, Cl and S input via serpentinite in subduction zones: implications for the nature of the fluid released at depth. *Terra Nova* 26, 96–101.
- Ernst, W.G., Liu, J., 1998. Experimental phase-equilibrium study of Al- and Ti-contents of calcic amphibole in MORB—a semiquantitative thermobarometer. *American Mineralogist* 83, 952–969.
- France, L., Ildefonse, B., Koepke, J., 2013. Hydrous magmatism triggered by assimilation of hydrothermally altered rocks in fossil oceanic crust (northern Oman ophiolite). *Geochemistry, Geophysics, Geosystems* 14, 2598–2614.
- Garofalo, P.S., 2012. The composition of Alpine marine sediments (Bündnerschiefer Formation, W Alps) and the mobility of their chemical components during orogenic metamorphism. *Lithos* 128–131, 55–72.
- Gilbert, M.C., Helz, R.T., Popp, R.K., Spear, F.S., 1982. Experimental studies of amphibole stability. *Mineralogical Society of America Reviews in Mineralogy* 9B, pp. 229–353.
- Gillis, K.M., Coogan, L.A., Chaussidon, M., 2003. Volatile element (B, Cl, F) behaviour in the roof of an axial magma chamber from the East Pacific Rise. *Earth and Planetary Science Letters* 213, 447–462.
- Grove, T.L., Chatterjee, N., Parman, S.W., Medard, E., 2006. The influence of H<sub>2</sub>O on mantle wedge melting. *Earth and Planetary Science Letters* 249, 74–89.
- Grove, T.L., Till, C.B., Lev, E., Chatterjee, N., Medard, E., 2009. Kinematic variables and water transport control the formation and location of arc volcanoes. *Nature* 459, 694–697.
- Guillot, S., Hattori, K., de Sigoyer, J., 2000. Mantle wedge serpentinization and exhumation of eclogites: insights from eastern Ladakh, northwest Himalaya. *Geology* 28, 199–202.
- Hart, S.R., Blusztajn, J., Dick, H.J.B., Meyer, P.S., Muehlenbachs, K., 1999. The fingerprint of seawater circulation in a 500-meter section of ocean crust gabbros. *Geochimica et Cosmochimica Acta* 63, 4059–4080.
- Holloway, J.G., Ford, C.E., 1975. Fluid absent melting of the fluorohydroxy-amphibole pargasite to 35 kilobars. *Earth and Planetary Science Letters* 25, 44–48.
- Ito, E.W., Harris, D.M., Anderson, A.T.J., 1983. Alteration of oceanic crust and geological cycling of chlorine and water. *Geochimica et Cosmochimica Acta* 47, 1613–1624.
- John, T., Scambelluri, M., Frische, M., Barnes, J.D., Bach, W., 2011. Dehydration of subducting serpentinite: implications for halogen mobility in subduction zones and the deep halogen cycle. *Earth and Planetary Science Letters* 308, 65–76.
- Kendrick, M.A., Woodhead, J., Kamenetsky, V., 2012. Tracking halogens through the subduction cycle. *Geology* 40, 1075–1078.
- Kendrick, M.A., Scambelluri, M., Honda, M., Phillips, D., 2011. High abundances of noble gas and chlorine delivered to the mantle by serpentinite subduction. *Nature Geosciences* 4, 807–812.
- Konrad-Schmolke, M., O'Brien, P.J., Zack, T., 2011. Fluid migration above a subducted slab—constraints on amount, pathways and major element mobility from partially overprinted eclogite-facies rocks. *Journal of Petrology* 52, 457–486.
- Konzett, J., Frost, D.J., 2009. The high P-T stability of hydroxyl-apatite in natural and simplified MORB—an experimental study to 15 GPa with implications for transport and storage of phosphorus and halogens in subduction zones. *Journal of Petrology* 50, 2043–2062.
- Koga, K., Garrido, C.J., Padrón-Navarta, J.A., López Sánchez-Vizcaino, V., Gómez-Pugnaire, M.T., 2014. FTIR and Raman spectroscopy characterization of fluorine-bearing titanite clinohumite in antigorite serpentinite and chlorite harzburgite. *Earth, Planets and Space* 66, 60.

- Lafay, R., Deschamps, F., Schwartz, S., Guillot, S., Godard, M., Debret, B., Nicollet, C., 2013. High-pressure serpentinites, a trap-and-release system controlled by metamorphic conditions: example from the Piedmont zone of the western Alps. *Chemical Geology* 343, 38–54.
- Lagabrielle, Y., Cannat, M., 1990. Alpine Jurassic ophiolites resemble to the modern central Atlantic basement. *Geology* 18, 319–322.
- Lagabrielle, Y., Polino, R., 1988. Un schéma structural du domaine des Schistes lustrés ophiolitifère au nord-ouest du massif du Mont Viso (Alpes Sud-Occidentales) et ses implications. *Comptes Rendus de l'Académie des Sciences* 306, 921–928.
- Lagabrielle, Y., Polino, R., Auzende, J.M., Blanchet, R., Caby, R., Fudral, S., Lemoine, M., Mével, C., Ohnenstetter, M., Robert, D., Tricart, P., 1984. Les témoins d'une tectonique intra-océanique dans le domaine téthysien: analyse des rapports entre les ophiolites et leurs couvertures métasédimentaires dans la zone piémontaise des Alpes franco-italiennes. *Ophioliti* 9, 67–88.
- Lagabrielle, Y., Vitale Brovarone, A., Ildefonse, B., 2014. Fossil Oceanic Core Complexes recognized in the blueschist ophiolitic units of Western Alps and Corsica. *Earth Science Reviews*. <http://dx.doi.org/10.1016/j.earscirev.2014.11.004>.
- Lemoine, M., Tricart, P., Boillot, G., 1987. Ultramafic and gabbroic ocean floor of the Ligurian Tethys (Alps, Corsica, Apennines). in search of a genetic model. *Geology* 15, 622–625.
- Le Voyer, M., Rose-Koga, E.F., Shimizu, N., Grove, T.L., Schiano, P., 2010. Two contrasting H<sub>2</sub>O-rich components in primary melt inclusions from Mount Shasta. *Journal of Petrology* 51, 1571–1595.
- Li, Y.H., 1991. Distribution patterns of the elements in the ocean: a synthesis. *Geochimica et Cosmochimica Acta* 55, 3223–3240.
- Li, Y.H., 1982. A brief discussion on the mean oceanic residence time of elements. *Geochimica et Cosmochimica Acta* 46, 2,671–2,675.
- Lombardo, B., Nervo, R., Compagnoni, R., Messiga, B., Kienast, J.R., Mével, C., et al., 1978. Osservazioni preliminari sulle ophioliti metamorfiche del monviso (Alpi occidentali). *Rendiconti della Società Italiana di Mineralogia e Petrologia* 34, 253–305.
- Manatschal, G., Sauter, D., Karpoff, A.M., Masini, E., Mohn, G., Lagabrielle, Y., 2011. The Chenaillet Ophiolite in the French/Italian Alps: an ancient analogue for an Oceanic Core Complex? *Lithos* 124, 169–184.
- Marschall, H.R., Pogge von Strandmann, P.A.E., Seitz, H.M., Elliott, T., Niu, Y., 2007. The lithium isotopic composition of orogenic eclogites and deep subducted slabs. *Earth and Planetary Science Letters* 262, 563–580.
- Marschall, H.R., Altherr, R., Gmüling, K., Kasztovszky, Z., 2009. Lithium, boron and chlorine as tracers for metasomatism in high-pressure metamorphic rocks: a case study from Syros (Greece). *Mineralogy and Petrology* 95, 291–302.
- Magni, V., Bouilhol, P., van Hunen, J., 2014. Deep water recycling through time. *Geochemistry, Geophysics, Geosystems*. <http://dx.doi.org/10.1002/2014GC005525>.
- McDonough, W.F., Sun, S., 1995. The composition of Earth. *Chemical Geology* 120, 223–253.
- Messiga, B., Scambelluri, M., Piccardo, G.B., 1995. Chloritoid-bearing assemblages in mafic systems and eclogite-facies hydration of alpine Mg–Al metagabbros (Erro-Tobbio Unit, Ligurian western Alps). *European Journal of Mineralogy* 7, 1149–1167.
- Messiga, B., Tribuzio, R., 1991. The reaction between olivine and plagioclase as a consequence of fluid-rock interactions during sub-seafloor metamorphism (Al–Mg gabbros, Northern Apennine ophiolites, Italy). *Schweizerische Mineralogische und Petrographische Mitteilungen* 71, 405–414.
- Mével, C., Caby, R., Kienast, J.R., 1978. Amphibolite facies conditions in oceanic crust: example of amphibolitized flaser gabbros and amphibolites from the Chenaillet ophiolite massif (Hautes Alpes, France). *Earth and Planetary Science Letters* 39, 98–108.
- Müntener, O., Manatschal, G., Desmurs, L., Pettke, T., 2010. Plagioclase peridotites in ocean–continent transitions: refertilized mantle domains generated by melt stagnation in the shallow mantle lithosphere. *Journal of Petrology* 51, 255–294.
- Nash, W.P., 1976. Fluorine, chlorine and OH-bearing minerals in the Skaergaard intrusion. *American Journal of Science* 276, 545–556.
- Oberti, R., Ungaretti, L., Cannillo, E., Hawthorne, F.C., 1993. The mechanism of Cl incorporation in amphibole. *American Mineralogist* 78, 746–752.
- Orberger, B., Métrich, N., Mosbah, M., Mével, C., Fouquet, Y., 1999. Nuclear microprobe analysis of serpentine from the mid-Atlantic ridge. *Nuclear Instruments and Methods in Physics Research B* 158, 575–581.
- Pawley, A.R., Holloway, J.R., 1993. Water sources for subduction zone volcanism: new experimental constraints. *Sciences* 260, 664–667.
- Penniston-Dorland, S.C., Sorensen, S.S., Ash, R.D., Khadke, S.V., 2010. Lithium isotopes as a tracer of fluids in a subduction zone mélange: Franciscan Complex, CA. *Earth and Planetary Science Letters* 292, 181–190.
- Penniston-Dorland, S.C., Bebout, G.E., Pogge von Strandmann, P.A.E., Elliott, T., Sorensen, S.S., 2012. Lithium and its isotopes as tracers of subduction zone fluids and metasomatic processes: evidence from the Catalina Schist, California, USA. *Geochimica et Cosmochimica Acta* 77, 530–545.
- Philippon, P., Agrinier, P., Scambelluri, M., 1998. Chlorine cycling during subduction of altered oceanic crust. *Earth and Planetary Science Letters* 161, 33–44.
- Poli, S., Schmidt, M.W., 2002. Petrology of subducted slabs. *Annual Review of Earth and Planetary Sciences* 30, 207–235.
- Poli, S., Schmidt, M.W., 1995. Water transport and release in subduction zones: experimental constraints on basaltic and andesitic systems. *Journal of Geophysical Research* 100, 22299–22314.
- Rose-Koga, E.F., Koga, K.T., Hamada, M., Héluouis, T., Whitehouse, M.J., Shimizu, N., 2014. Volatile (F and Cl) concentrations in Iwate olivine-hosted melt inclusions indicating low-temperature subduction. *Earth, Planets and Space* 66, 81.
- Salters, V.J.M., Stracke, A., 2004. Composition of the depleted mantle. *Geochemistry, Geophysics, Geosystems* 5. <http://dx.doi.org/10.1029/2003GC000597>.
- Sano, T., Miyoshi, M., Ingle, S., Banerjee, N.R., Ishimoto, M., Fukuoka, T., 2008. Boron and chlorine contents of upper oceanic crust: basement samples from IODP Hole 1256D. *Geochemistry, Geophysics, Geosystems* 9. <http://dx.doi.org/10.1029/2008GC002182>.
- Scambelluri, M., Fiebig, J., Malaspina, N., Müntener, O., Pettke, T., 2004a. Serpentinite subduction: implications for fluid processes and trace-element recycling. *International Geology Review* 46, 595–613.
- Scambelluri, M., Müntener, O., Ottolini, L., Pettke, T.T., Vannucci, R., 2004b. The fate of B, Cl and Li in the subducted oceanic mantle and in the antigorite breakdown fluids. *Earth and Planetary Science Letters* 222, 217–234.
- Scambelluri, M., Tonarini, S., 2012. Boron isotope evidence for shallow fluid transfer across subduction zones by serpentinized mantle. *Geology* 40, 907–910.
- Schmidt, M.W., Poli, S., 2014. Devolatilization during subduction. *Treatise on Geochemistry*. <http://dx.doi.org/10.1016/B978-0-08-095975-7.00321-1>.
- Schwartz, S., Allemand, P., Guillot, S., 2001. Numerical model of the effect of serpentinites on the exhumation of eclogitic rocks: insights from the Monviso ophiolitic massif (Western Alps). *Tectonophysics* 42, 193–206.
- Schwartz, S., Guillot, S., Reynard, B., Lafay, R., Debret, B., Nicollet, C., Lanari, P., Auzende, A.L., 2013. Pressure-temperature estimates of the lizardite/antigorite transition in high pressure serpentinites. *Lithos* 178, 197–210.
- Shaw, A.M., Behn, M.D., Humphris, S.E., Sohn, R.A., Gregg, P.M., 2010. Deep pooling of low degree melts and volatile fluxes at the 85°E segment of the Gakkel Ridge: evidence from olivine-hosted melt inclusions and glasses. *Earth and Planetary Science Letters* 289, 311–322.
- Selverstone, J., Sharp, Z.D., 2015. Chlorine isotope behavior during prograde metamorphism of sedimentary rocks. *Earth and Planetary Science Letters* 417, 120–131.
- Straub, S.M., Layne, G.D., 2003. The systematics of chlorine, fluorine, and water in Izu arc front volcanic rocks: implications for volatile recycling in subduction zones. *Geochimica et Cosmochimica Acta* 67, 4179–4203.
- Spear, F.S., 1993. *Metamorphic phase equilibria and pressure–temperature–time paths*. Mineralogical Society of America, Washington, D.C (799 pp.).
- Tribuzio, R., Riccardi, M.P., Ottolini, L., 1995. Trace element redistribution in high-temperature deformed gabbros from East Ligurian ophiolites (Northern Apennines, Italy): constraints on the origin of syndeformation fluids. *Journal of Metamorphic Geology* 13, 367–377.
- Tricart, P., 1984. From passive margin to continental collision: a tectonic scenario for the western Alps. *American Journal of Science* 284, 97–120.
- Tricart, P., Lemoine, M., 1986. From faulted blocks to megamullions and megaboudins—Tethyan heritage in the structure of the western Alps. *Tectonics* 5, 95–118.
- Tricart, P., Schwartz, S., 2006. A north–south section across the Queyras Schistes lustrés (Piedmont zone, Western Alps): syncollisional refolding of a subduction wedge. *Eclogae Geologicae Helveticae* 99, 429–442.
- Ulmer, P., Trommsdorff, V., 1995. Serpentinite stability to mantle depths and subduction related magmatism. *Science* 268, 858–861.
- Van den Bleeken, G., Koga, K.T., 2015. Experimentally determined distribution of fluorine and chlorine upon hydrous slab melting, and implications for F–Cl cycling through subduction zones. *Geochimica et Cosmochimica Acta* 171, 353–373.
- Vanko, D.A., 1986. High-chlorine amphiboles from oceanic rocks: product of highly saline hydrothermal fluids? *American Mineralogist* 71, 51–59.
- Vils, F., Pelletier, L., Kalt, A., Müntener, O., Ludwig, T., 2008. The lithium, boron and beryllium content of serpentinized peridotites from ODP Leg 209 (Sites 1272A and 1274A): implications for lithium and boron budgets of oceanic lithosphere. *Geochimica et Cosmochimica Acta* 72, 5475–5504.
- Vils, F., Müntener, O., Kalt, A., Ludwig, T., 2010. Implications of the serpentine phase transition on the behaviour of beryllium and lithium–boron of subducted ultramafic rocks. *Geochimica et Cosmochimica Acta* 75, 1249–1271.
- Vitale Brovarone, A., Beyssac, O., Alard, O., Martin, L., Picatto, M., 2014. Lawsonite metasomatism and trace element recycling in subduction zones. *Journal of Metamorphic Geology* 32, 498–514.
- Volfinger, M., Robert, J.-L., Vielzeuf, D., Neiva, A.M.R., 1985. Structural control of the chlorine content of OH-bearing silicates (micas and amphiboles). *Geochimica et Cosmochimica Acta* 49, 37–48.
- Wedepohl, K.H., Hartmann, G., 1994. The composition of the primitive upper earth's mantle. In: Meyer, H.O.A., Leonardos, O.H. (Eds.), *Kimberlites, related rocks and mantle xenoliths*. Companhia de Pesquisa de Recursos Minerais, Rio de Janeiro 1, pp. 486–495.
- Wünder, B., Schreyer, W., 1997. Antigorite: high pressure stability in the system MgO–SiO<sub>2</sub>–H<sub>2</sub>O (MSH). *Lithos* 41, 213–227.
- Wünder, B., Deschamps, F., Watenphul, A., Guillot, S., Meixner, A., Romer, R.L., Wirth, R., 2010. The effect of chrysotile nanotubes on the serpentine–fluid Li–isotopic fractionation. *Contributions to Mineralogy and Petrology* 159, 781–790.
- Zack, T., Tomaschak, P.B., Rudnick, R.L., Dalpé, C., McDonough, W.F., 2003. Extremely light Li in orogenic eclogites: the role of isotope fractionation during dehydration in subducted oceanic crust. *Earth and Planetary Science Letters* 208, 279–290.